Impact of electron correlations on the nonlinear Edelstein effect

Jun Ōiké* and Robert Peters
Department of Physics, Kyoto University, Kyoto 606-8502, Japan

(Received 31 March 2024; revised 8 August 2024; accepted 10 September 2024; published 3 October 2024)

Nonlinear spintronics, which combines nonlinear dynamics with spintronics, opens a new route for controlling spin and spin dynamics beyond conventional spintronics based on linear responses. Electron correlations can lead to a large nonlinear response and thus may play a key role in nonlinear spintronics. This paper focuses on the nonlinear Edelstein effect (NEE) and examines the impact of electron correlations on the NEE through numerical calculations on a Hubbard model. We find that electron correlations can either enhance or suppress the nonlinear response. Specifically, the enhancement and suppression are due to the real and imaginary components of self-energy, respectively. In addition, the NEE is closely related to photomagnetic and optomagnetic effects. Our findings demonstrate that electron correlations can either enhance or suppress the optical spin injection, depending on light frequencies, whereas always strengthening the inverse Faraday effect.

DOI: 10.1103/PhysRevB.110.165111

I. INTRODUCTION

Electric generation and control of spin degrees of freedom are central issues in modern spintronics [1–3]. A typical technique is to utilize the linear Edelstein effect (LEE), where an electric field $\boldsymbol{E}$ induces a nonequilibrium spin density $\delta\boldsymbol{s}$ in noncentrosymmetric metals: $\delta\boldsymbol{s} \propto \boldsymbol{E}$. The LEE was first theoretically proposed in Refs. [4,5] and was experimentally realized in GaAs [6–8]. Furthermore, a spin torque driven by the LEE was theoretically proposed in magnetic semiconductors [9–11] and a current-induced domain inversion was observed in GaMnAs [12]. These findings have triggered increased attention to the LEE in the field of spintronics.

Interestingly, the literature concerning the LEE deals almost exclusively with noninteracting systems such as topological insulators [13–18], Weyl semimetals [19–22], and superconductors [23–28]; only a few works analyzed electron correlations by using Fermi liquid theory or dynamical mean-field theory (DMFT) [29–32]. One reason for ignoring electron correlations is that conventional spintronics is based on linear responses. Reference [33], for example, has demonstrated that correlation effects do not strongly affect a linear response. On the other hand, some theoretical calculations [33–36] and experimental results [37–41] have shown that electron correlations can lead to a large nonlinear response. Thus, electron correlations may play a key role in nonlinear spintronics.

Recently, nonlinear responses have also been considered in the field of spintronics. Of particular interest is the nonlinear Edelstein effect (NEE) [42–48], which is characterized by $\delta\boldsymbol{s} \propto \boldsymbol{E}^2$. The NEE significantly influences the spin response from the following three points. First, the NEE has no restrictions on spatial inversion ($\mathcal{P}$). Because spin is an axial vector, but electric fields are polar vectors, the LEE only appears in noncentrosymmetric materials. On the other hand, the NEE also exists in centrosymmetric systems, which account for approximately 80% of all materials. Second, the NEE can also be observed in semiconductors and insulators, unlike the LEE [47,48]. This is because optical transition can generate a static spin density in the same way as the bulk photovoltaic effect generates a static electric polarization [49–51]. Thus, the NEE is divided into the current-induced NEE in metals [42–44] and the light-induced NEE in metals, semiconductors, and insulators [45–48]. Note that here we define the static response in nonmagnetic materials as the Edelstein effect, regardless of whether they are metals or insulators. The static response in magnets is the magnetoelectric effect [52–54]. Third, the NEE can have a sizable magnitude despite its nonlinear nature. With a moderate electric field, the strength of the NEE can exceed that of the LEE in transition-metal dichalcogenides [47] and common transition metals [42,43]. The criterion is $E = 10^5 \sim 10^7$ V/m, which is readily feasible in experiments [12]. Due to these properties, the NEE is essential to the development of nonlinear spintronics.

In this work, we study the impact of electron correlations on the NEE by performing numerical calculations on a Hubbard model. First, we formulate the NEE at finite temperatures on the basis of a diagrammatic approach [33,55–58]. This formulation allows us to derive an equation based on single-particle Green's functions. The self-energy of the Green's function includes correlation effects, which enables us to consider electron correlations. Then, we use DMFT [59] to obtain the self-energy of the model and calculate the NEE incorporating electron correlations. Our results show that electron correlations enhance the current-induced NEE, but can either enhance or suppress the light-induced NEE. The enhancement and suppression originate from the real and imaginary parts of self-energy, respectively.

The light-induced NEE is related to photomagnetic and optomagnetic effects, which are studied in the field of magneto-optics. Thus, we examine the interaction dependence of these

*Contact author: oike.jun.32y@st.kyoto-u.ac.jp

effects. Specifically, we focus on the optical spin injection [1,60] as a photomagnetic effect and the inverse Faraday effect (IFE) [61,62] as an optomagnetic effect. Our findings show that electron correlations can either enhance or suppress the optical spin injection, depending on light frequencies. On the other hand, electron correlations strengthen the IFE regardless of light frequencies.

The rest of this paper is organized as follows: In Sec. II, we introduce the formulation of the NEE to the second order in electric fields. Section III A presents the details of the Hubbard model, and Sec. III B shows the self-energy and spectral functions of the model. We then show the interaction dependence of the current-induced NEE in Sec. IV A and the light-induced NEE in Sec. IV B. Section V is devoted to discussing the results of the previous section. We first reveal the origin of the enhancement and suppression of the responses in Secs. V A and V B. We then discuss the interaction dependence of the optical spin injection and the IFE in Sec. V C. Finally, Sec. VI summarizes this work and gives a future outlook.

II. FORMULATION

We first introduce the definition of the NEE. The spin density induced by an electric field is written in the frequency domain as

$$\begin{aligned}\langle \delta\hat{s}_\alpha(\omega_\Sigma)\rangle = &\int \frac{d\omega_1}{2\pi}\zeta^{(1)}_{\alpha;\beta}(\omega_\Sigma;\omega_1)E^\beta(\omega_1)2\pi\delta_{\omega_1,\omega_\Sigma}\\ &+\int\frac{d\omega_1}{2\pi}\frac{d\omega_2}{2\pi}\zeta^{(2)}_{\alpha;\beta\gamma}(\omega_\Sigma;\omega_1,\omega_2)E^\beta(\omega_1)\\ &\times E^\gamma(\omega_2)2\pi\delta_{\omega_1+\omega_2,\omega_\Sigma}+\cdots,\end{aligned} \tag{1}$$

where $\zeta^{(n)}_{\alpha;\alpha_1\ldots\alpha_n}(\omega_\Sigma;\omega_1,\ldots,\omega_n)$ is the nth-order response function, and the Greek indices label Cartesian components. The variable ω_Σ corresponds to the frequency of the generated spin and ω_i corresponds to the frequency of the electric field. In this study, we focus on the static response ($\omega_\Sigma = 0$) recognized as the Edelstein effect. The first term on the right-hand side of Eq. (1) represents the LEE and the other terms describe the NEE. In particular, the second-order NEE is divided into two cases,

$$\zeta^{(2)}_{\alpha;\beta\gamma} \coloneqq \lim_{\omega_1,\omega_2\to 0}\zeta^{(2)}_{\alpha;\beta\gamma}(\omega_\Sigma;\omega_1,\omega_2), \tag{2}$$

$$\zeta^{(2)}_{\alpha;\beta\gamma}(\Omega) \coloneqq \zeta^{(2)}_{\alpha;\beta\gamma}(0;\Omega,-\Omega), \tag{3}$$

where Ω is the frequency of the incident light. Equation (2) describes the current-induced NEE and Eq. (3) describes the light-induced NEE. To calculate these two types of NEE, we then formulate the second-order response function using the path-integral Matsubara formalism.

The response function is obtained by taking a functional derivative of the partition function of a perturbed system. Thus, our first step is to construct the perturbed Hamiltonian from an unperturbed Hamiltonian,

$$\hat{H}(\boldsymbol{k}) = \hat{H}_0(\boldsymbol{k}) + \hat{H}_{\rm int}, \tag{4}$$

where $\hat{H}_0(\boldsymbol{k})$ is a noninteracting Hamiltonian and $\hat{H}_{\rm int}$ is the two-particle interacting part of the Hamiltonian. Throughout this paper, we suppose only a local interaction, which does not depend on momentum $\boldsymbol{k}$. We then consider the interaction between a carrier and an electromagnetic field. Here, we assume the electric dipole approximation, under which the electromagnetic field is approximated by a uniform electric field, $\boldsymbol{E}(t)$. This uniformity limits the gauge degree of freedom to either the length or velocity gauge. Here, we adopt the velocity gauge, where we treat the effect of the electric field by rewriting Eq. (4) as

$$\begin{aligned}\hat{H}(\boldsymbol{k}) &\to \hat{H}\left[\boldsymbol{k}-\frac{q}{\hbar}\boldsymbol{A}(t)\right]\\ &= \hat{H}(\boldsymbol{k}) + \sum_{n=1}^{\infty}\frac{1}{n!}\left\{\prod_{i=1}^{n}\left[-\frac{q}{\hbar}A^{\alpha_i}(t)\partial_{k_{\alpha_i}}\right]\right\}\hat{H}(\boldsymbol{k}),\end{aligned} \tag{5}$$

where $\boldsymbol{E}(t) = -\partial\boldsymbol{A}(t)/\partial t$, $\partial_{k_{\alpha_i}} = \partial/\partial k_{\alpha_i}$, $\hbar$ is the Planck constant, and q is the charge of the carrier. We perform the Taylor expansion around the vector potential $\boldsymbol{A}(t)$ in the second line of Eq. (5) to capture the nonlinear response. Furthermore, we include an auxiliary term, $\hat{H}_{\rm B} = -\boldsymbol{B}(t)\cdot\hat{\boldsymbol{s}}$, in Eq. (4) to obtain the spin response. The field $\boldsymbol{B}(t)$ is the conjugate field of spin $\hat{\boldsymbol{s}}$ and is taken to zero after the variation. Note that one can derive a similar formulation for other physical quantities by replacing $\hat{\boldsymbol{s}}$ and $\boldsymbol{B}(t)$ with the quantity of interest, $\hat{\boldsymbol{\theta}}$, and its conjugate field, respectively. However, $\hat{\boldsymbol{\theta}}$ must be a local operator that is well defined in periodic systems, such as the spin operator $\hat{\boldsymbol{s}}$.

Then, we derive the second-order response function from the partition function of the perturbed system. This partition function is written in the path-integral formalism as

$$Z[A,B] = \int \mathcal{D}\bar{\psi}\mathcal{D}\psi\exp[-S[A,B]], \tag{6}$$

where $\bar{\psi}$ and ψ are fermionic creation and annihilation operators represented by Grassmann numbers, $\mathcal{D}\psi$ denotes a path-integral measure that goes over all possible field values, and $S[A,B]$ is the action of the system in imaginary time τ. This action is described as

$$\begin{aligned}S[A,B] = \int_0^\beta d\tau\Bigg[&\sum_{\lambda,\eta}\int\frac{d\boldsymbol{k}}{(2\pi)^d}\bar{\psi}_{\boldsymbol{k}\lambda}(\tau)\Big\{(\partial_\tau-\mu)\delta_{\lambda\eta}\\ &+H_0^{\lambda\eta}\left[\boldsymbol{k}-\frac{q}{\hbar}\boldsymbol{A}(\tau)\right]-\boldsymbol{B}(\tau)\cdot\boldsymbol{s}^{\lambda\eta}\Big\}\psi_{\boldsymbol{k}\eta}(\tau)+H_{\rm int}\Bigg],\end{aligned} \tag{7}$$

where $\partial_\tau = \partial/\partial\tau$, $\beta = 1/k_{\rm B}T$ with the temperature T and the Boltzmann constant $k_{\rm B}$, d is the dimension of the system, μ is the chemical potential, and $X^{\lambda\eta}$ is the matrix representation of an operator $\hat{X}$. The expectation value of the spin density is expressed by a functional derivative as [63]

$$\langle\delta\hat{s}_\alpha(\tau)\rangle = \left.\frac{\delta}{\delta B^\alpha(\tau)}\right|_{B=0}\ln Z[A,B]. \tag{8}$$

We then expand $Z[A,B]$ in powers of the vector potential $\boldsymbol{A}(\tau)$ and define the nth-order response function, $\chi^{(n)}_{\alpha;\alpha_1\ldots\alpha_n}(\tau;\tau_1,\ldots,\tau_n)$, as the coefficient to

$A^{\alpha_1}(\tau_1)\ldots A^{\alpha_n}(\tau_n)$. As a result, we obtain

$$\chi^{(n)}_{\alpha;\alpha_1\ldots\alpha_n}(\tau;\tau_1,\ldots,\tau_n) = \frac{1}{Z[0]}\left(\prod_{i=1}^{n}\frac{\delta}{\delta A^{\alpha_i}(\tau_i)}\right)\frac{\delta}{\delta B^{\alpha}(\tau)}\bigg|_{B=A=0} Z[A,B]. \quad (9)$$

We further express the second-order response function with single-particle Green's functions. Taking the Fourier transformation to Matsubara frequencies and performing an analytic continuation, we obtain

$$\begin{aligned}\zeta^{(2)}_{\alpha;\beta\gamma}(\omega_\Sigma;\omega_1,\omega_2) &= \frac{\hbar}{(\omega_1+i\delta)(\omega_2+i\delta)}\int\frac{d\boldsymbol{k}}{(2\pi)^d}\int_{-\infty}^{\infty}\frac{d\omega}{2\pi i}\\ &\times f(\omega)\mathrm{Tr}\big[s_\alpha G^R(\boldsymbol{k},\omega+\omega_\Sigma)g^R_{\beta\gamma}(\boldsymbol{k},\omega+\omega_2)G^{R-A}(\boldsymbol{k},\omega)\\ &+ s_\alpha G^R(\boldsymbol{k},\omega+\omega_1)g^{R-A}_{\beta\gamma}(\boldsymbol{k},\omega)G^A(\boldsymbol{k},\omega-\omega_2)\\ &+ s_\alpha G^{R-A}(\boldsymbol{k},\omega)g^A_{\beta\gamma}(\boldsymbol{k},\omega-\omega_1)G^A(\boldsymbol{k},\omega-\omega_\Sigma)\big]\\ &+ [(\beta,\omega_1)\leftrightarrow(\gamma,\omega_2)], \end{aligned} \quad (10)$$

where $g^a_{\beta\gamma}(\boldsymbol{k},\omega)$ is given by

$$g^a_{\beta\gamma}(\boldsymbol{k},\omega) = \begin{cases} J_\beta(\boldsymbol{k})G^a(\boldsymbol{k},\omega)J_\gamma(\boldsymbol{k})+\frac{1}{2}J_{\beta\gamma}(\boldsymbol{k}) & \text{for } a=R,A\\ J_\beta(\boldsymbol{k})G^a(\boldsymbol{k},\omega)J_\gamma(\boldsymbol{k}) & \text{for } a=R-A. \end{cases} \quad (11)$$

Here, $f(\omega)=[1+\exp(\beta\hbar\omega)]^{-1}$ is the Fermi distribution function, $G^{R/A}(\boldsymbol{k},\omega)$ is a retarded/advanced Green's function, $J_{\alpha_1\ldots\alpha_n}(\boldsymbol{k})=(q/\hbar)^n\partial_{k_{\alpha_1}}\ldots\partial_{k_{\alpha_n}}H_0(\boldsymbol{k})$ is a current operator, and $G^{R-A}=G^R-G^A$. The symbol $[(\beta,\omega_1)\leftrightarrow(\gamma,\omega_2)]$ corresponds to the interchange of these indices and frequencies. Note that we redefine the nth-order response function, $\zeta^{(n)}_{\alpha;\alpha_1\ldots\alpha_n}(\omega_\Sigma;\omega_1,\ldots,\omega_n)$, as the coefficient to $E^{\alpha_1}(\omega_1)\ldots E^{\alpha_n}(\omega_n)$, using the relation $\boldsymbol{E}(\omega_j)=i(\omega_j+i\delta)\boldsymbol{A}(\omega_j)$. The infinitesimal value $\delta>0$ is an adiabatic factor of the external field and is taken to zero after calculation. Additionally, we ignore the vertex correction in the occurring many-particle Green's functions, which enables us to describe the response function as the product of single-particle Green's functions. The details of the derivation are given in Appendix A. Correlation effects are incorporated through the self-energy $\Sigma^{R/A}(\omega)$ of the Green's function, $G^{R/A}(\boldsymbol{k},\omega)=[\hbar\omega-H_0(\boldsymbol{k})+\mu-\Sigma^{R/A}(\omega)\pm i\eta]^{-1}$, where $\eta>0$ is an adiabatic factor of the Green's function. Throughout this paper, we ignore the momentum dependence of self-energy by an approximation of DMFT [59]. Thus, ignoring vertex correction does not break the generalized Ward identity [64]. On the other hand, if self-energy includes momentum dependence, the inclusion of vertex correction is necessary to satisfy the generalized Ward identity.

From Eq. (10), we can calculate the current-induced NEE and the light-induced NEE. For the current-induced NEE, however, we need to avoid the divergence that occurs in the low-frequency region. Correctly taking the DC limit, $\omega_1,\omega_2\to 0$, we can rewrite Eq. (10) as

$$\begin{aligned}\zeta^{(2)}_{\alpha;\beta\gamma} &= -2\hbar\int\frac{d\boldsymbol{k}}{(2\pi)^d}\int_{-\infty}^{\infty}\frac{d\omega}{2\pi}\\ &\times\left(-\frac{\partial f(\omega)}{\partial\omega}\mathrm{Im}\left\{\mathrm{Tr}\left[s_\alpha\frac{\partial G^R(\boldsymbol{k},\omega)}{\partial\omega}g^R_{\beta\gamma}(\boldsymbol{k},\omega)G^A(\boldsymbol{k},\omega)\right]\right\}\right.\\ &\left.-f(\omega)\mathrm{Im}\left\{\mathrm{Tr}\left[s_\alpha\frac{\partial}{\partial\omega}\left(\frac{\partial G^R(\boldsymbol{k},\omega)}{\partial\omega}g^R_{\beta\gamma}(\boldsymbol{k},\omega)\right)G^R(\boldsymbol{k},\omega)\right]\right\}\right)\\ &+(\beta\leftrightarrow\gamma), \end{aligned} \quad (12)$$

which is derived in Appendix B.

We additionally comment on relevant previous studies. For the light-induced NEE, an expression similar to Eq. (10) was derived by using the Keldysh formalism [65,66]. In addition, we reproduce results of the semiclassical approach [42,53] and the reduced density matrix (RDM) formalism [48] by taking the weak-scattering limit for Eqs. (10) and (12), which is given in Appendices C and D.

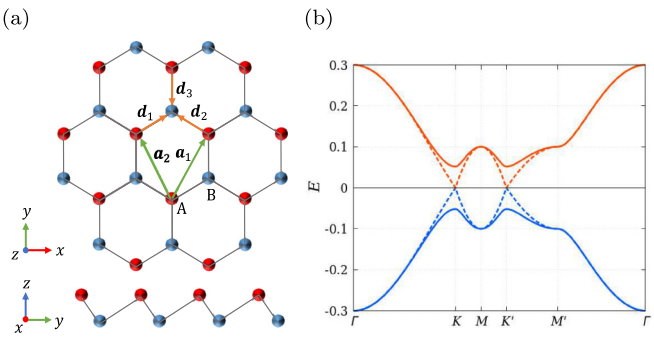

FIG. 1. (a) Top and side views of a buckled two-dimensional honeycomb lattice. The green solid arrows indicate lattice vectors, and the orange solid arrows indicate vectors connecting between nearest-neighbor sites. (b) Energy dispersion of the model at $U=0$ for $(t,t_{\mathrm{R}})=(0.1,0.01)$. The solid lines show the dispersion for $t_{\mathrm{so}}=0.1$, and the dashed lines show the dispersion for $t_{\mathrm{so}}=0.0$.

III. MODEL AND METHOD

A. Model

We consider a Kane-Mele-Hubbard (KMH) model defined on a buckled two-dimensional honeycomb lattice [Fig. 1(a)]. The Hamiltonian takes the form

$$\begin{aligned}\hat{H} &= -t\sum_{\langle ij\rangle,\sigma}\hat{c}^\dagger_{i\sigma}\hat{c}_{j\sigma}+it_{\mathrm{so}}\sum_{\langle\langle ij\rangle\rangle,\sigma\sigma'}\nu_{ij}\hat{c}^\dagger_{i\sigma}\sigma^z_{\sigma\sigma'}\hat{c}_{j\sigma'}\\ &- it_{\mathrm{R}}\sum_{\langle\langle ij\rangle\rangle,\sigma\sigma'}\mu_{ij}\hat{c}^\dagger_{i\sigma}(\boldsymbol{\sigma}\times\boldsymbol{d}_{ij})^z_{\sigma\sigma'}\hat{c}_{j\sigma'}+U\sum_i\hat{n}_{i\uparrow}\hat{n}_{i\downarrow}, \end{aligned} \quad (13)$$

where the noninteracting part is based on a Kane-Mele model [42,67–69] and belongs to the D_{3d} point group. Here, $\hat{c}^\dagger_{i\sigma}$ and $\hat{c}_{i\sigma}$ are creation and annihilation operators of electrons with the spin $\sigma=\{\uparrow,\downarrow\}$ at a site i, $\hat{n}_{i\sigma}=\hat{c}^\dagger_{i\sigma}\hat{c}_{i\sigma}$ is the number operator, and $\sum_{\langle ij\rangle}$ and $\sum_{\langle\langle ij\rangle\rangle}$ denote the sums over the nearest-neighbor (NN) and next-nearest-neighbor (NNN)

sites, respectively. The first term represents the NN hopping with hopping strength t. The second term represents the intrinsic spin-orbit coupling (SOC) with coupling strength $t_{\rm so}$ between NNN electrons. Here, σ^z is the z component of the Pauli matrix $\boldsymbol{\sigma}$ and $\nu_{ij} = +\ (-)$ when an electron moves counterclockwise (clockwise) around a hexagon. The third term represents the Rashba SOC with coupling strength $t_{\rm R}$ between NNN electrons. Here, $\boldsymbol{d}_{ij}$ is a unit vector pointing from the jth site to the ith site, and $\mu_{ij} = +\ (-)$ for A (B) sites. This term originates in the lattice buckling, resulting in symmetry reduction from D_{6h} to D_{3d}. The visualization of the lattice buckling is shown in Fig. 1(a). The last term represents a Hubbard-like on-site interaction with interaction strength U.

In momentum space, the noninteracting part is given by

$$\hat{H}_0 = \sum_{\boldsymbol{k},\sigma} [\eta(\boldsymbol{k}) \hat{c}^\dagger_{\boldsymbol{k}A\sigma} \hat{c}_{\boldsymbol{k}B\sigma} + \text{H.c.}] + \sum_{\boldsymbol{k},ss',\sigma\sigma'} \boldsymbol{g}(\boldsymbol{k}) \cdot \boldsymbol{\sigma}_{\sigma\sigma'} \tau^z_{ss'} \hat{c}^\dagger_{\boldsymbol{k}s\sigma} \hat{c}_{\boldsymbol{k}s'\sigma'}, \tag{14}$$

where $\hat{\Psi}_{\boldsymbol{k}} = (\hat{c}_{\boldsymbol{k}A\uparrow}, \hat{c}_{\boldsymbol{k}A\downarrow}, \hat{c}_{\boldsymbol{k}B\uparrow}, \hat{c}_{\boldsymbol{k}B\downarrow})^\top$ is the basis with momentum $\boldsymbol{k}$ and the spin $\sigma = \{\uparrow, \downarrow\}$ on two sublattices, $s =$ A, B, and $\boldsymbol{\sigma}$ ($\boldsymbol{\tau}$) is the Pauli matrix for the spin (sublattice) degrees of freedom. The coefficients are defined as

$$\eta(\boldsymbol{k}) = -t \sum_{i=1}^{3} e^{i\boldsymbol{k}\cdot\boldsymbol{d}_i}, \tag{15}$$

$$g_x(\boldsymbol{k}) = \sqrt{3} t_{\rm R} (\sin \boldsymbol{k} \cdot \boldsymbol{a}_1 + \sin \boldsymbol{k} \cdot \boldsymbol{a}_2), \tag{16}$$

$$g_y(\boldsymbol{k}) = -t_{\rm R} [\sin \boldsymbol{k} \cdot \boldsymbol{a}_1 - \sin \boldsymbol{k} \cdot \boldsymbol{a}_2 + 2 \sin \boldsymbol{k} \cdot (\boldsymbol{a}_1 - \boldsymbol{a}_2)], \tag{17}$$

$$g_z(\boldsymbol{k}) = 2 t_{\rm so} [\sin \boldsymbol{k} \cdot \boldsymbol{a}_1 - \sin \boldsymbol{k} \cdot \boldsymbol{a}_2 - \sin \boldsymbol{k} \cdot (\boldsymbol{a}_1 - \boldsymbol{a}_2)], \tag{18}$$

where $\boldsymbol{a}_1 = (\sqrt{3}a/2, 3a/2)$ and $\boldsymbol{a}_2 = (-\sqrt{3}a/2, 3a/2)$ are lattice vectors, $\boldsymbol{d}_1 = (\sqrt{3}a/2, a/2)$, $\boldsymbol{d}_2 = (-\sqrt{3}a/2, a/2)$, and $\boldsymbol{d}_3 = (0, -a)$ are vectors connecting between NN sites, and a is the lattice constant. Equation (15) is responsible for linear dispersions at the K and K' points (Dirac points), similar to graphene. Equations (16) and (17) represent the sublattice-dependent antisymmetric SOC in a locally noncentrosymmetric system. The locally noncentrosymmetric system lacks $\mathcal{P}$ symmetry at the site level, but the global $\mathcal{P}$ symmetry is preserved by interchanging the sublattices [31,67,70–72]. Specifically, the site symmetry is denoted by a noncentrosymmetric point group C_{3v} and the global symmetry belongs to a centrosymmetric point group D_{3d}. Equation (18) represents the SOC that opens gaps at the Dirac points, as shown in Fig. 1(b).

In the numerical calculations, we use the following parameters: $(t, t_{\rm so}, t_{\rm R}, T) = (0.1, 0.01, 0.01, 0.001)$, and set $\hbar = q = k_{\rm B} = a = 1$. Furthermore, we use the basis that satisfies

$$\hat{H}_0(\boldsymbol{k}) |u_n(\boldsymbol{k})\rangle = \varepsilon_n(\boldsymbol{k}) |u_n(\boldsymbol{k})\rangle, \tag{19}$$

where $|u_n(\boldsymbol{k})\rangle$ is the periodic part of the Bloch state and $\varepsilon_n(\boldsymbol{k})$ is the eigenvalue labeled by the crystal momentum $\boldsymbol{k}$ in the first Brillouin zone. The other index, $n = (n, i_n)$, denotes a band n and the spinor index, $i_n = 1, 2$. The matrix representation of an operator $\hat{X}$ under this basis is given by

$$X^{nm}(\boldsymbol{k}) = \langle u_n(\boldsymbol{k}) | \hat{X} | u_m(\boldsymbol{k}) \rangle = [U(\boldsymbol{k})^{-1} X U(\boldsymbol{k})]^{nm}, \tag{20}$$

where $U(\boldsymbol{k})$ is a unitary matrix diagonalizing the noninteracting Hamiltonian $H_0(\boldsymbol{k})$, and X on the rightmost side denotes the matrix representation under the basis $\hat{\Psi}_{\boldsymbol{k}}$. As a specific example, the spin operator is given by

$$\boldsymbol{s}^{nm}(\boldsymbol{k}) = \frac{\hbar}{2} \left[U(\boldsymbol{k})^{-1} \begin{pmatrix} \boldsymbol{\sigma} & 0 \\ 0 & \boldsymbol{\sigma} \end{pmatrix} U(\boldsymbol{k}) \right]^{nm}, \tag{21}$$

where $\boldsymbol{\sigma}$ is the Pauli matrix for each sublattice. In the following, we will often omit the $\boldsymbol{k}$ index of an operator $X(\boldsymbol{k})$ to enhance readability.

B. Dynamical mean-field theory

The role of DMFT is to map an original lattice problem onto a self-consistent quantum impurity problem [59]. This mapping is performed by calculating the local Green's function,

$$G(\omega) = \int \frac{d\boldsymbol{k}}{(2\pi)^d} [\hbar\omega - H_0(\boldsymbol{k}) + \mu - \Sigma(\omega) + i\eta]^{-1}. \tag{22}$$

The local Green's function satisfies the following self-consistent equation:

$$g^{-1}(\omega) = G^{-1}(\omega) + \Sigma(\omega), \tag{23}$$

where $g(\omega)$ denotes the coupling of a quantum impurity to a bath of conduction electrons. Here, we use the numerical renormalization group [73,74] to solve the quantum impurity problem and find the self-consistent solution of the KMH model.

In this study, we assume a homogeneous paramagnetic state to focus on the NEE defined as a spin response in paramagnetic systems. Accordingly, we neglect any possible spin and sublattice dependence of the self-energy. However, we note that the homogeneous paramagnetic phase is the energetically stable state only for $U/t < 4$ in KMH-like models [75,76]. For larger interaction strengths, a magnetically ordered state becomes the stable state. The same behavior might apply to this KMH model. Nevertheless, we calculate the NEE for interaction strengths above this critical value, noting that the paramagnetic state might be only metastable at these strengths.

First, we show the imaginary and real parts of the self-energy of the KMH model at half filling in Figs. 2(a) and 2(b), respectively. The imaginary part of the self-energy becomes large with increasing interaction. The real part of the self-energy represents the renormalization effect of the quasiparticles. The renormalization factor is defined as

$$Z = \left(1 - \frac{1}{\hbar} \frac{\partial \mathrm{Re}\Sigma(\omega)}{\partial \omega} \bigg|_{\omega=0} \right)^{-1}, \tag{24}$$

where $Z^{-1} > 1$ for correlated electron systems. We see the enhancement of the renormalization effect with increasing interaction in Fig. 2(b).

Then, we show spectral functions of the KMH model at half filling in Fig. 2(c) and in an electron-doped regime in

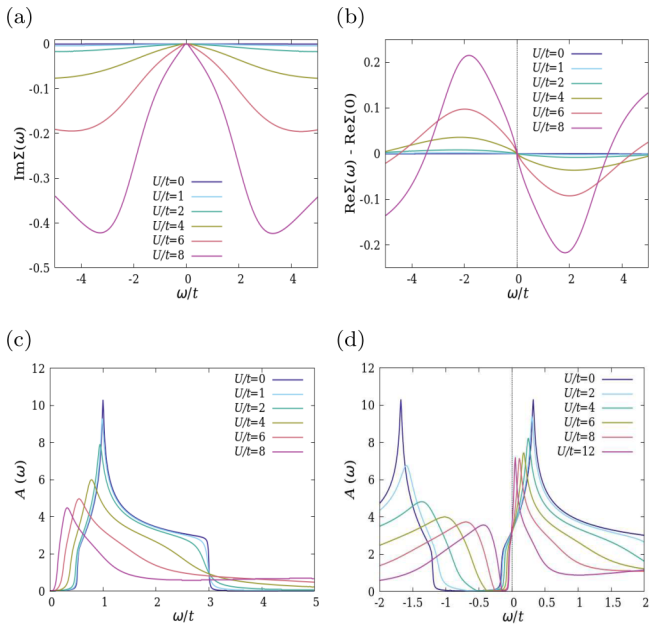

FIG. 2. (a),(b) Self-energy at half filling for different interaction strengths U/t from 0 to 8. The left and right figures show the imaginary and real parts of the self-energy, respectively. We shift the real part of the self-energy by $-\mathrm{Re}\Sigma(0)$. (c),(d) Spectral functions, (c) at half filling and (d) in an electron-doped regime for different U/t from 0 to 12. We show only the $\omega/t > 0$ region in (c) because of particle-hole symmetry. We set the electron density to $\langle n\rangle = 1.097$ in (d).

Fig. 2(d). The spectral function is defined via the Green's function as

$$A(\omega) = -\frac{1}{\pi}\int \frac{d\boldsymbol{k}}{(2\pi)^d}\mathrm{Im}G^R(\boldsymbol{k},\omega). \tag{25}$$

To visualize the spectral functions, we use $\eta = 0.001$ for both cases. Note that during the DMFT self-consistent cycle, we use $\eta = 0.01$ at half filling and $\eta = 0.02$ in the doped regime to improve the convergence. As interaction increases, the peak is gradually suppressed, and the spectral weight continuously shifts to higher energy because of the imaginary part of the self-energy. Meanwhile, the peak position moves closer to the Fermi energy because of the renormalization of the band structure. These behaviors are characteristic of correlated electron systems. In the following, we calculate the current-induced NEE in the electron-doped regime and the light-induced NEE at half filling. Note that the current-induced NEE vanishes at half filling because the system is an insulator.

IV. RESULTS

First, we discuss the symmetry constraints of the NEE. The NEE tensor obeys the following symmetry transformation rule:

$$\zeta^{(2)}_{\alpha';\beta'\gamma'} = \det(\mathcal{R})\mathcal{R}_{\alpha'\alpha}\mathcal{R}_{\beta'\beta}\mathcal{R}_{\gamma'\gamma}\zeta^{(2)}_{\alpha;\beta\gamma}, \tag{26}$$

where $\mathcal{R}$ is a point group operation. This response tensor is divided into the symmetric component $\mathcal{S}_{\alpha;\beta\gamma}$ and the antisymmetric component $\mathcal{A}_{\alpha;\beta\gamma}$, regarding the incident electric field:

$$\mathcal{S}_{\alpha;\beta\gamma} = \left(\zeta^{(2)}_{\alpha;\beta\gamma} + \zeta^{(2)}_{\alpha;\gamma\beta}\right)/2, \tag{27}$$

$$\mathcal{A}_{\alpha;\beta\gamma} = \left(\zeta^{(2)}_{\alpha;\beta\gamma} - \zeta^{(2)}_{\alpha;\gamma\beta}\right)/2. \tag{28}$$

Reference [42] has clarified the symmetry constraints of the symmetric part. According to this literature, the symmetry of the KMH model, $\mathcal{D}_{3d}$, allows for the following symmetric components: $\mathcal{S}_{x;yy} = \mathcal{S}_{y;xy} = -\mathcal{S}_{x;xx}$. The antisymmetric part for the KMH model includes $\mathcal{A}_{x;xy} = \mathcal{A}_{y;xy} = 0$ and the nonvanishing component $\mathcal{A}_{z;xy}$.

Then, we consider whether the current-induced NEE tensor and light-induced NEE tensor are symmetric or antisymmetric. Obviously, the current-induced NEE tensor is symmetric. The light-induced NEE is further classified into the responses under linearly polarized light (LPL) and circularly polarized light (CPL). Using a relation $\boldsymbol{E}(\Omega) = \boldsymbol{E}^*(-\Omega)$, we extract the LPL and CPL components from the light-induced NEE [72],

$$\langle\delta\hat{s}_\alpha\rangle = \int \frac{d\Omega}{2\pi}\zeta^{(2)}_{\alpha;\beta\gamma}(\Omega)E^\beta(\Omega)E^\gamma(-\Omega) \to \begin{cases}\langle\delta\hat{s}_\alpha\rangle_{\mathrm{LPL}}\\ \langle\delta\hat{s}_\alpha\rangle_{\mathrm{CPL}},\end{cases} \tag{29}$$

where $\langle\delta\hat{s}_\alpha\rangle_{\mathrm{LPL}}$ represents the LPL-induced NEE and $\langle\delta\hat{s}_\alpha\rangle_{\mathrm{CPL}}$ represents the CPL-induced NEE. Specifically, they are given by

$$\langle\delta\hat{s}_\alpha\rangle_{\mathrm{LPL}} = \int \frac{d\Omega}{2\pi}\eta^{(2)}_{\alpha;\beta\gamma}(\Omega)L^{\beta\gamma}(\Omega), \tag{30}$$

$$\langle\delta\hat{s}_\alpha\rangle_{\mathrm{CPL}} = \int \frac{d\Omega}{2\pi}\varepsilon_{\beta\gamma\delta}\xi^{(2)}_{\alpha;\beta\gamma}(\Omega)C^\delta(\Omega), \tag{31}$$

where $L^{\beta\gamma}(\Omega) = \mathrm{Re}\{E^\beta(\Omega)[E^\gamma(\Omega)]^*\}$ and $\boldsymbol{C}(\Omega) = \frac{i}{2}\boldsymbol{E}(\Omega)\times\boldsymbol{E}^*(\Omega)$ are the LPL and CPL components of the product of the electric fields, respectively. The coefficients are given by

$$\eta^{(2)}_{\alpha;\beta\gamma}(\Omega) = \tfrac{1}{2}\mathrm{Re}\left\{\zeta^{(2)}_{\alpha;\beta\gamma}(\Omega) + \zeta^{(2)}_{\alpha;\gamma\beta}(\Omega)\right\}, \tag{32}$$

$$\xi^{(2)}_{\alpha;\beta\gamma}(\Omega) = \tfrac{1}{2}\mathrm{Im}\left\{\zeta^{(2)}_{\alpha;\beta\gamma}(\Omega) - \zeta^{(2)}_{\alpha;\gamma\beta}(\Omega)\right\}, \tag{33}$$

which denote the LPL-induced NEE tensor and the CPL-induced NEE tensor, respectively. Thus, the LPL-induced NEE tensor is symmetric and the CPL-induced NEE tensor is antisymmetric. In the following, we calculate the xyy component for the current-induced NEE and the LPL-induced NEE, and the zxy component for the CPL-induced NEE.

A. Current-induced NEE

Figure 3(a) shows the interaction dependence of the current-induced NEE. The orange and blue lines indicate the contributions of the Fermi surface and Fermi sea terms in Eq. (12), respectively. The response from the Fermi surface terms increases with increasing interaction, whereas the response from the Fermi sea terms becomes zero. We first discuss this difference. The current-induced NEE requires breaking time-reversal ($\mathcal{T}$) symmetry because spin is odd

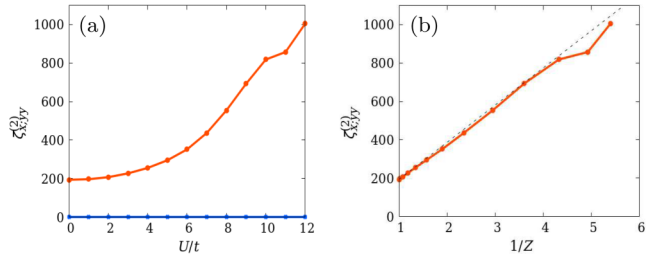

FIG. 3. Magnitude of the calculated current-induced NEE over (a) U/t and (b) $1/Z$. The orange and blue lines in (a) and (b) indicate the contributions of the Fermi surface and Fermi sea terms, respectively. The dashed line in (b) corresponds to $\zeta^{(2)}_{x;yy} = Z^{-1}\zeta^{(2),\mathrm{free}}_{x;yy}$, where $\zeta^{(2),\mathrm{free}}_{x;yy}$ denotes $\zeta^{(2)}_{x;yy}$ at $U/t = 0.0$.

under $\mathcal{T}$, but electric fields are even. Dissipation due to impurity scattering breaks $\mathcal{T}$ symmetry in nonmagnetic materials. However, such dissipation does not appear in Fermi sea terms because the electrons below Fermi surfaces are not free to move. Thus, the contribution of the Fermi sea terms becomes zero [see Fig. 3(a)] and we ignore these terms in the following. Then, we replot the result in Fig. 3(b) by replacing the horizontal axis with the inverse of the renormalization factor. The dashed line represents

$$\zeta^{(2)}_{x;yy} = Z^{-1}\zeta^{(2),\mathrm{free}}_{x;yy}, \tag{34}$$

where $\zeta^{(2),\mathrm{free}}_{x;yy}$ denotes $\zeta^{(2)}_{x;yy}$ at $U/t = 0.0$. The response follows the dashed line and is thus enhanced by Z^{-1} compared to noninteracting systems. This enhancement agrees with previous results showing that the renormalization effect enhances the nonlinear DC conductivity to the same extent [33,36].

B. Light-induced NEE

Figure 4(a) shows the interaction dependence of the LPL-induced NEE. A single peak appears in each spectrum and takes a maximal value. As interaction increases, the peak magnitude gradually increases and the peak position shifts toward the low-frequency region. Then, we replot the result in Fig. 4(b) by using the renormalized frequency Ω/Z on the horizontal axis and analyze the influence of the renormalization. The peaks originate in the same interband transition and electron correlations enhance its contribution. The degree of the enhancement is shown in Fig 4(c), which displays the magnitudes of the peaks at $\Omega/Z = 0.15$ over the renormalization parameter. However, the magnitudes are not enhanced by the factor of Z^{-1}, unlike the current-induced NEE.

More interesting is the interaction dependence of the CPL-induced NEE, which is shown in Fig. 4(d). Three peaks appear in each spectrum and their peak positions imply the contributions from interband transitions around the K, M, and Γ points [see Fig. 1(b)]. Interaction effect is different for these peaks: the peak at the lowest frequency is enhanced by interaction, whereas the peaks at the higher energies are suppressed.

V. DISCUSSION

In this section, we discuss the results of the previous section. First, we analytically show that the renormalization

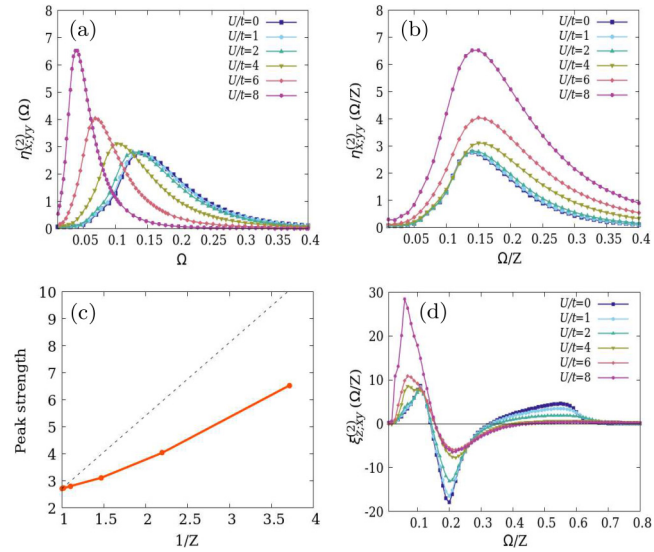

FIG. 4. (a)–(c) Calculated LPL-induced NEE. (a),(b) Interaction dependence of the response over Ω and Ω/Z, respectively. (c) Interaction dependence of the peak at $\Omega/Z = 0.15$ in (b). The dashed line corresponds to $\eta^{(2)}_{x;yy}(\Omega/Z) = Z^{-1}\eta^{(2),\mathrm{free}}_{x;yy}(\Omega/Z)$ at $\Omega/Z = 0.15$, where $\eta^{(2),\mathrm{free}}_{x;yy}$ denotes $\eta^{(2)}_{x;yy}$ at $U/t = 0.0$. (d) Calculated CPL-induced NEE over Ω/Z for different interaction strengths.

effect enhances the current-induced NEE by Z^{-1} in Sec. V A. Furthermore, we discuss the weak degree of the enhancement for the light-induced NEE. Then, we explain the complex frequency dependence exhibited by the CPL-induced NEE in Sec. V B. Finally, in Sec. V C, we comment on the interaction dependence of photomagnetic and optomagnetic effects related to the light-induced NEE.

A. Origin of the increased response and factor of the weak degree of the enhancement

Current-induced responses are mainly generated at the Fermi energy ($\omega = 0$). Self-energy is expanded in the vicinity of the Fermi energy as

$$\Sigma^R(\omega) \simeq \mathrm{Re}\Sigma^R(0) + \hbar\omega\frac{\partial \mathrm{Re}\Sigma^R(\omega)}{\hbar\partial\omega}\bigg|_{\omega=0} + i\mathrm{Im}\Sigma^R(0). \tag{35}$$

This expansion allows us to divide the Green's function into the coherent part G^R_{coh} and the incoherent part G^R_{inc} as

$$G^R(\omega) = G^R_{\mathrm{coh}}(\omega) + G^R_{\mathrm{inc}}(\omega), \tag{36}$$

$$G^R_{\mathrm{coh}}(\omega) = \frac{Z}{\hbar\omega - Z\varepsilon' + i\Gamma}, \tag{37}$$

where $\varepsilon' = \varepsilon - \mu + \mathrm{Re}\Sigma^R(0)$ and $\Gamma = -Z\mathrm{Im}\Sigma^R(0)$. The coherent part expresses quasiparticles with energy ε' and lifetime $\hbar/\Gamma$. We note that Γ is very small in our calculations. Supposing that a Green's function is expressed only by its coherent part and that Γ is sufficiently small, we can describe the Green's function as

$$G^R(\omega) = G^{R,\mathrm{free}}(Z^{-1}\omega), \tag{38}$$

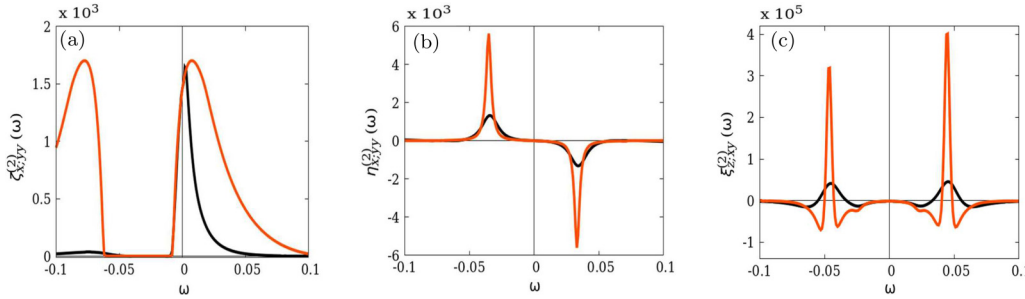

FIG. 5. Frequency-resolved response functions at $U/t = 6$ for (a) the current-induced NEE, (b) the LPL-induced NEE ($\Omega/Z = 0.15$), and (c) the CPL-induced NEE ($\Omega/Z = 0.20$). The black line indicates the contribution of the full Green's function and the orange line indicates the contribution of the coherent part.

where $G^{R,\text{free}}$ is a Green's function for noninteracting systems. Following the same procedure as Ref. [33], we find

$$\zeta^{(2)}_{\alpha;\beta\gamma} \approx Z^{-1}\zeta^{(2),\text{free}}_{\alpha;\beta\gamma}, \tag{39}$$

where $\zeta^{(2),\text{free}}_{\alpha;\beta\gamma}$ is the response function for noninteracting systems. Equation (39) states that the renormalization effect enhances the current-induced NEE by Z^{-1}. Consequently, large interaction strengths with a large renormalization effect result in a large response [see Figs. 2(b) and 3(b)]. Obviously, this enhancement is due to the real part of the self-energy. On the other hand, Eq. (35) is not valid for the light-induced NEE because of the frequency dependence of the self-energy. Nevertheless, we cannot explain the increased response of the light-induced NEE without the renormalization effect. Accordingly, to evaluate the contribution of the coherent part, we calculate the frequency-resolved response function $\zeta^{(2)}_{\alpha;\beta\gamma}(\omega)$, which is defined as

$$\zeta^{(2)}_{\alpha;\beta\gamma} = \int \frac{d\omega}{2\pi} F(\omega)\zeta^{(2)}_{\alpha;\beta\gamma}(\omega), \tag{40}$$

where $F(\omega) = -\partial f(\omega)/\partial\omega$ for the current-induced NEE, and $F(\omega) = f(\omega)$ for the light-induced NEE.

Figures 5(a)–5(c) show the frequency-resolved response functions for the current-induced NEE, the LPL-induced NEE, and the CPL-induced NEE, respectively. The black line indicates the contribution of the full Green's function and the orange line indicates the contribution of the coherent part. For the current-induced NEE, the contribution of the coherent part near the Fermi energy is identical to the total contribution. On the other hand, for the light-induced NEE, the coherent part overestimates the total response. Therefore, the light-induced NEE is not as strongly enhanced as the current-induced NEE because of the frequency dependence of the self-energy.

B. Complex frequency dependence exhibited by the CPL-induced NEE

We analyze the CPL-induced NEE by using the Bloch basis and Eq. (21). We first divide Eq. (10) into the diagonal part [$\propto s^{nn}_{\alpha}(\boldsymbol{k})$] and the off-diagonal part [$\propto s^{nm}_{\alpha}(\boldsymbol{k})$], and then calculate the response for each part. Figures 6(a) and 6(b) show the contributions of the diagonal and off-diagonal parts, respectively. Although the main contribution comes from the diagonal part, the response from the off-diagonal part is also finite. Most importantly, electron correlations enhance the off-diagonal response, whereas the diagonal response is suppressed for the large frequencies. Here, we note that the diagonal response is an intraband effect, which depends on extrinsic scattering time. On the other hand, the off-diagonal response is an interband effect, which is intrinsic and only depends on light frequencies. These can be confirmed in Eq. (54) of Ref. [48]. Furthermore, the LPL-induced NEE is also an interband effect, as seen in Eq. (53) of Ref. [48]. Therefore, reduction of the lifetime due to electron correlations can suppress dissipative responses, such as the diagonal response of the CPL-induced NEE. To verify this hypothesis, we recalculate the CPL-induced NEE by effectively excluding the imaginary part of the self-energy, which reflects dissipation.

Figures 6(c) and 6(d) show the results for the diagonal and off-diagonal parts, respectively. The second peak of Fig. 6(c) is indeed enhanced when we neglect the imaginary part of the self-energy. This result indirectly shows that the imaginary part suppresses the response. Moreover, the second peak of Fig. 6(a) is strongly suppressed at the large interaction

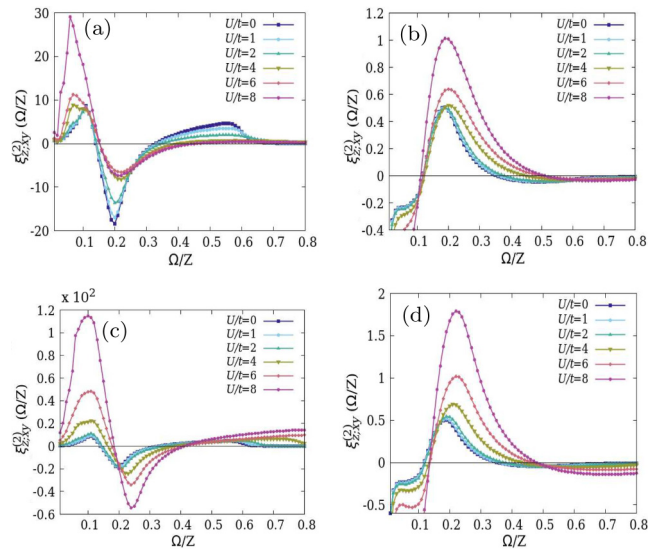

FIG. 6. CPL-induced NEE calculated by including or neglecting the imaginary part of the self-energy. The upper panels show the NEE including the imaginary part for (a) the diagonal part and (b) the off-diagonal part. The lower panels show the NEE neglecting the imaginary part for (c) the diagonal part and (d) the off-diagonal part.

strengths because of the increased imaginary part with increasing interaction [see Figs. 2(a) and 6(a)]. On the other hand, the off-diagonal response does not include the suppression by the imaginary part. Comparing Figs. 6(b) and 6(d), we can see that the real part of the self-energy is sufficient to explain the NEE.

Besides the suppression by the imaginary part, the diagonal response is enhanced by the real part of the self-energy, which creates the complex frequency dependence. For example, the first peak in the low-frequency region is enhanced because the renormalization effect of the real part exceeds the suppression effect of the imaginary part. On the other hand, the suppression effect is stronger for the peaks at the larger frequencies [see Fig. 6(a)]. Furthermore, the frequency dependence of the real part explains why some peak positions in the low-frequency region shift to the smaller frequencies. The renormalization effect of the real part is weaker for larger frequencies. Together with the suppression effect of the imaginary part, this leads to a shift in the peak positions for the large interaction strengths [compare Figs. 6(a) and 6(c)].

C. Interaction dependence of photomagnetic and optomagnetic effects

Photomagnetic and optomagnetic effects are nonthermal phenomena, where light changes the magnetic properties of materials, but does not involve the heating of electrons by laser pulses [62]. Photomagnetic effects depend on photon absorption and are associated with the optical spin injection [1,60]. Optomagnetic effects do not require photon absorption and are related to the IFE [61] and the inverse Cotton-Mouton effect (ICME) [77].

The optical spin injection generates a finite spin expectation value of electrons by transferring the angular momentum of photons during optical excitation induced by CPL. Using band representation, we see that the optical spin injection corresponds to the diagonal response of the CPL-induced NEE [47,48,78]. This correspondence can also be confirmed from Fig. 6(a): the peak positions suggest the presence of optical excitation induced by CPL. Therefore, we conclude that electron correlations can either enhance or suppress the optical spin injection, depending on light frequencies.

The IFE and ICME generate effective magnetic fields under CPL and LPL, respectively. According to Ref. [47], these effects are described as

$$H^{\gamma}_{\mathrm{IFE}} \propto a_{\alpha\beta\gamma}\{E^{\alpha}(\Omega)[E^{\beta}(\Omega)]^{*} - E^{\beta}(\Omega)[E^{\alpha}(\Omega)]^{*}\}, \quad (41)$$

$$H^{\gamma}_{\mathrm{ICME}} \propto b_{\alpha\beta\gamma\delta}M^{\delta}\{E^{\alpha}(\Omega)[E^{\beta}(\Omega)]^{*} + E^{\beta}(\Omega)[E^{\alpha}(\Omega)]^{*}\}, \quad (42)$$

where $\boldsymbol{H}_{\mathrm{IFE/ICME}}$ is an effective magnetic field for the IFE/ICME, $\boldsymbol{M}$ is a magnetization, and $a_{\alpha\beta\gamma}$ and $b_{\alpha\beta\gamma\delta}$ are phenomenological parameters. The IFE and ICME look at the same effect as the light-induced NEE because spin density excited by light generates an effective magnetic field. These responses require breaking $\mathcal{T}$ symmetry similarly to the current-induced NEE. However, different $\mathcal{T}$ properties of LPL and CPL lead to different results for the IFE and ICME when we focus on their interaction dependence.

TABLE I. Response characteristics on the NEE to incident electric fields: The real and imaginary parts of self-energy enhance (↗) and suppress (↘) the response, respectively. The symbol ✓/× means the existence (✓) or absence (×) of each effect. Furthermore, we use ✓̸ when each effect is possible but not as large as ✓.

Self-energy	Effect on the response	Current	LPL	CPL
Real	↗	✓	✓̸	✓̸
Imaginary	↘	×	×	✓

Basically, LPL does not inherently break $\mathcal{T}$ symmetry because the oscillation directions of LPL do not change under $\mathcal{T}$. Accordingly, energy dissipation associated with interband transitions induced by LPL breaks $\mathcal{T}$ symmetry in nonmagnetic materials. However, the ICME is an equilibrium phenomenon and thus finite only in magnets, which can be confirmed from Eq. (42). On the other hand, the LPL-induced NEE involves interband transitions and takes a finite value even in nonmagnetic materials, as shown in Fig. 4(b). Therefore, the ICME does not correspond to the LPL-induced NEE in nonmagnetic materials and we cannot conclude whether electron correlations enhance or suppress the ICME.

Unlike LPL, CPL inherently breaks $\mathcal{T}$ symmetry because the helicities of CPL change under $\mathcal{T}$. Thus, the IFE can have a finite value in nonmagnetic materials, unlike the ICME. Notably, the IFE corresponds to the off-diagonal response of the CPL-induced NEE. Indeed, Fig. 6(b) shows that the off-diagonal response generates a nonzero value even in the nonresonant-frequency region ($\Omega/Z \ll 0.10$), indicating its independence from photon absorption. Therefore, we conclude that electron correlations enhance the IFE regardless of light frequencies.

VI. SUMMARY AND OUTLOOK

We have analyzed the impact of electron correlations on the NEE in a nonmagnetic system. Specifically, we have formulated the NEE using a full quantum mechanical approach and have performed numerical calculations on a Hubbard model. The NEE consists of three types: the current-induced NEE, the LPL-induced NEE, and the CPL-induced NEE. Then, we have found that electron correlations can either enhance or suppress the nonlinear responses. The enhancement is due to the renormalization effect, which originates in the real part of the self-energy. On the other hand, the suppression only occurs in dissipative responses and depends on the imaginary part of self-energy. Specifically, the current-induced NEE and the LPL-induced NEE only include the real-part effect, whereas the CPL-induced NEE includes both the real-part and imaginary-part effects. However, we found that the light-induced NEE is not as strongly enhanced as the current-induced NEE because of the frequency dependence of the self-energy. Finally, Table I summarizes the effects of self-energy on the different types of NEE.

Then, we have examined the interaction dependence of the optical spin injection, the IFE, and the ICME, which are related to the light-induced NEE. The optical spin injection and the IFE correspond to the diagonal and off-diagonal responses of the CPL-induced NEE, respectively. The

diagonal response includes both the real-part and imaginary-part effects, whereas the off-diagonal response only includes the real-part effect. Therefore, electron correlations can either enhance or suppress the optical injection, depending on light frequencies, whereas always strengthening the IFE. On the other hand, we cannot discuss the interaction dependence of the ICME because the ICME does not necessarily correspond to the LPL-induced NEE. In addition, we stress that the above analyses focus on an insulator. The light-induced NEE in metals has another intraband effect originating from a Fermi surface contribution [48]. Therefore, the response in metals might show more complex interaction dependence. We will leave these open questions as future work.

Note added. Recently, Kodama *et al.* have experimentally detected the current-induced nonlinear magnetoelectric effect on a Pt-Py bilayer [79]. Their study suggests that one can experimentally capture the current-induced NEE in correlated electron systems. In addition, the equations formulated in this study enable quantitative evaluation by combining first-principles calculations with DMFT. This capability will give a material platform for correlated electron spintronics mediated by nonlinear responses.

ACKNOWLEDGMENTS

J.O. is grateful to Koki Shinada and Taisei Kitamura for their valuable comments. R.P. is supported by JSPS KAKENHI Grant No. JP23K03300. Parts of the numerical simulations in this work have been done using the facilities of the Supercomputer Center at the Institute for Solid State Physics, the University of Tokyo.

APPENDIX A: DERIVATION OF THE RESPONSE FUNCTION BASED ON THE PATH-INTEGRAL MATSUBARA FORMALISM

The derivation of Eq. (10) in the main text consists of four main steps. We also derive the first-order response function for reference and omit $\int d\boldsymbol{k}/(2\pi)^d$ for brevity.

First, we express the response functions in terms of Matsubara Green's functions. The response functions are expressed by the functional derivatives as

$$\chi^{(1)}_{\alpha;\beta}(\tau;\tau_1) = \frac{1}{Z[0]}\frac{\delta}{\delta A^\beta(\tau_1)}\frac{\delta}{\delta B^\alpha(\tau)}\bigg|_{B=A=0} Z[A,B] = \sum_{\lambda,\eta,\sigma,\rho}\left\langle \bar\psi_\lambda(\tau) s^{\lambda\eta}_\alpha \psi_\eta(\tau)\bar\psi_\sigma(\tau_1) J^{\sigma\rho}_\beta \psi_\rho(\tau_1)\right\rangle, \tag{A1}$$

$$\begin{aligned}\chi^{(2)}_{\alpha;\beta\gamma}(\tau;\tau_1,\tau_2) &= \frac{1}{Z[0]}\frac{\delta}{\delta A^\gamma(\tau_2)}\frac{\delta}{\delta A^\beta(\tau_1)}\frac{\delta}{\delta B^\alpha(\tau)}\bigg|_{B=A=0} Z[A,B] = -\delta(\tau_1-\tau_2)\sum_{\lambda,\eta,\sigma,\rho}\left\langle \bar\psi_\lambda(\tau) s^{\lambda\eta}_\alpha \psi_\eta(\tau)\bar\psi_\sigma(\tau_1) J^{\sigma\rho}_{\beta\gamma} \psi_\rho(\tau_1)\right\rangle \\ &+ \sum_{\lambda,\eta,\sigma,\rho,\mu,\nu}\left\langle \bar\psi_\lambda(\tau) s^{\lambda\eta}_\alpha \psi_\eta(\tau)\bar\psi_\sigma(\tau_1) J^{\sigma\rho}_\beta \psi_\rho(\tau_1)\bar\psi_\mu(\tau_2) J^{\mu\nu}_\gamma \psi_\nu(\tau_2)\right\rangle,\end{aligned} \tag{A2}$$

where $\delta(x)$ is the Dirac delta function, and $\langle X\rangle = Z[0]^{-1}\int \mathcal{D}\bar\psi\mathcal{D}\psi X e^{-S[0]}$ is a functional integral over an action without external fields. Using Wick's theorem and neglecting vertex correction, we can write these many-particle Green's functions as the product of single-particle Green's functions,

$$\chi^{(1)}_{\alpha;\beta}(\tau;\tau_1) = -\sum_{\lambda,\eta,\sigma,\rho} s^{\lambda\eta}_\alpha \langle -\psi_\eta(\tau)\bar\psi_\sigma(\tau_1)\rangle J^{\sigma\rho}_\beta \langle -\psi_\rho(\tau_1)\bar\psi_\lambda(\tau)\rangle, \tag{A3}$$

$$\begin{aligned}\chi^{(2)}_{\alpha;\beta\gamma}(\tau;\tau_1,\tau_2) &= \delta(\tau_1-\tau_2)\sum_{\lambda,\eta,\sigma,\rho} s^{\lambda\eta}_\alpha \langle -\psi_\eta(\tau)\bar\psi_\sigma(\tau_1)\rangle J^{\sigma\rho}_{\beta\gamma} \langle -\psi_\rho(\tau_1)\bar\psi_\lambda(\tau)\rangle \\ &+ \sum_{\lambda,\eta,\sigma,\rho,\mu,\nu}\left[s^{\lambda\eta}_\alpha \langle -\psi_\eta(\tau)\bar\psi_\sigma(\tau_1)\rangle J^{\sigma\rho}_\beta \langle -\psi_\rho(\tau_1)\bar\psi_\mu(\tau_2)\rangle J^{\mu\nu}_\gamma \langle -\psi_\nu(\tau_2)\bar\psi_\lambda(\tau)\rangle + [(\beta,\tau_1)\leftrightarrow(\gamma,\tau_2)]\right].\end{aligned} \tag{A4}$$

Note that the other terms vanish because they are proportional to the expectation value of a current operator in the absence of applied electric fields.

Second, we take the Fourier transformation to Matsubara frequencies,

$$\chi^{(1)}_{\alpha;\beta}(i\omega_n;i\omega_n) = -\frac{1}{\beta}\sum_{\omega_l}\mathrm{Tr}[s_\alpha \mathscr{G}(i\omega_l+i\omega_n)J_\beta \mathscr{G}(i\omega_l)], \tag{A5}$$

$$\begin{aligned}\chi^{(2)}_{\alpha;\beta\gamma}(i\omega_n+i\omega_m;i\omega_n,i\omega_m) &= \frac{1}{\beta}\sum_{\omega_l}\mathrm{Tr}\bigg[\frac{1}{2}s_\alpha \mathscr{G}(i\omega_l+i\omega_n+i\omega_m)J_{\beta\gamma}\mathscr{G}(i\omega_l) \\ &+ s_\alpha \mathscr{G}(i\omega_l+i\omega_n+i\omega_m)J_\beta \mathscr{G}(i\omega_l+i\omega_m)J_\gamma \mathscr{G}(i\omega_l)\bigg] + [(\beta,i\omega_n)\leftrightarrow(\gamma,i\omega_m)],\end{aligned} \tag{A6}$$

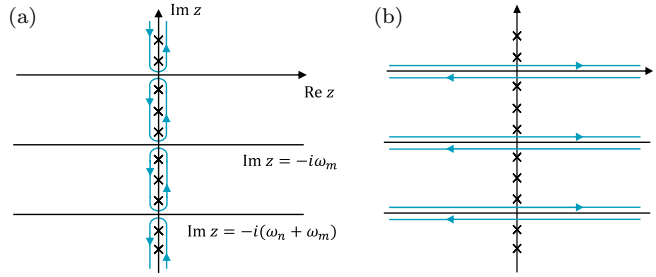

FIG. 7. (a) Locations of the poles (×) of $f(z)$ and integral paths (blue curves) around them. Each integral path does not span the different regions of the analyticity of $X(z)$. (b) Integral paths to sum over the Matsubara frequency. Each integral path is along the axis parallel to the real axis, at a distance of $\pm i\eta$ from the analytical boundary of $X(z)$. Note that the displayed paths correspond to using $X(z)$ as the second-order response function.

where $\omega_l = (2l+1)\pi/\beta$ is a fermionic Matsubara frequency, and $\omega_n = 2n\pi/\beta$ and $\omega_m = 2m\pi/\beta$ are bosonic Matsubara frequencies originating from photons. Here, we define $\mathcal{G}(\tau-\tau') = \langle -\psi(\tau)\bar{\psi}(\tau')\rangle$, and use $\mathcal{G}(\tau) = \beta^{-1}\sum_l \mathcal{G}(i\omega_l)e^{-i\omega_l\tau}$ and $\int_0^\beta e^{i(\omega_n-\omega_m)\tau} = \beta\delta_{nm}$.

Third, we perform the sum over the Matsubara frequency by using an identity $\beta^{-1}\sum_l X(i\omega_l) = -\oint_C \frac{dz}{2\pi i} f(z)X(z)$. The integral symbol $\oint_C$ represents paths that avoid the poles of $X(z)$ and only surround the poles of the Fermi distribution function, $f(z) = (1+e^{\beta z})^{-1}$ [Fig. 7(a)]. Because each path can be transformed within each regular region [Fig. 7(b)], the response functions are calculated by

$$\chi^{(1)}_{\alpha;\beta}(i\omega_n; i\omega_n) = \int_{-\infty}^{\infty}\frac{d\varepsilon}{2\pi i}f(\varepsilon)\mathrm{Tr}\{s_\alpha\mathcal{G}(\varepsilon+i\omega_n)J_\beta[\mathcal{G}(\varepsilon+i\eta)-\mathcal{G}(\varepsilon-i\eta)] + s_\alpha[\mathcal{G}(\varepsilon+i\eta)-\mathcal{G}(\varepsilon-i\eta)]J_\beta\mathcal{G}(\varepsilon-i\omega_n)\}, \tag{A7}$$

$$\begin{aligned}\chi^{(2)}_{\alpha;\beta\gamma}(i\omega_n+i\omega_m; i\omega_n, i\omega_m) = -\int_{-\infty}^{\infty}\frac{d\varepsilon}{2\pi i}f(\varepsilon)\mathrm{Tr}\Big\{&\frac{1}{2}\{s_\alpha\mathcal{G}(\varepsilon+i\omega_n+i\omega_m)J_{\beta\gamma}[\mathcal{G}(\varepsilon+i\eta)-\mathcal{G}(\varepsilon-i\eta)]\\ &+ s_\alpha[\mathcal{G}(\varepsilon+i\eta)-\mathcal{G}(\varepsilon-i\eta)]J_{\beta\gamma}\mathcal{G}(\varepsilon-i\omega_n-i\omega_m)\} + s_\alpha\mathcal{G}(\varepsilon+i\omega_n+i\omega_m)\\ &\times J_\beta\mathcal{G}(\varepsilon+i\omega_m)J_\gamma[\mathcal{G}(\varepsilon+i\eta)-\mathcal{G}(\varepsilon-i\eta)] + s_\alpha\mathcal{G}(\varepsilon+i\omega_n)J_\beta[\mathcal{G}(\varepsilon+i\eta)-\mathcal{G}(\varepsilon-i\eta)]\\ &\times J_\gamma\mathcal{G}(\varepsilon-i\omega_m) + s_\alpha[(\mathcal{G}(\varepsilon+i\eta)-\mathcal{G}(\varepsilon-i\eta)]J_\beta\mathcal{G}(\varepsilon-i\omega_n)J_\gamma\mathcal{G}(\varepsilon-i\omega_n-i\omega_m)\Big\}\\ &+ [(\beta, i\omega_n)\leftrightarrow(\gamma, i\omega_m)],\end{aligned} \tag{A8}$$

where η denotes an infinitesimal value and we use $f(\varepsilon-i\omega_n) = f(\varepsilon-i\omega_n-i\omega_m) = f(\varepsilon)$ and $i\omega_n, i\omega_m \gg i\eta$ to derive the final expressions.

Fourth, we perform an analytic continuation by $i\omega_n \to \hbar\omega_1 + i\eta$, $i\omega_m \to \hbar\omega_2 + i\eta$. Using that analytic functions in the upper/lower plane become retarded/advanced Green's functions, we describe the response functions as

$$\chi^{(1)}_{\alpha;\beta}(\omega_1;\omega_1) = \int_{-\infty}^{\infty}\frac{d\varepsilon}{2\pi i}f(\varepsilon)\mathrm{Tr}\{s_\alpha G^R(\varepsilon+\hbar\omega_1)J_\beta[G^R(\varepsilon)-G^A(\varepsilon)] + s_\alpha[G^R(\varepsilon)-G^A(\varepsilon)]J_\beta G^A(\varepsilon-\hbar\omega_1)\}, \tag{A9}$$

$$\begin{aligned}\chi^{(2)}_{\alpha;\beta\gamma}(\omega_\Sigma;\omega_1,\omega_2) = -\int_{-\infty}^{\infty}\frac{d\varepsilon}{2\pi i}f(\varepsilon)\Big(&\frac{1}{2}\mathrm{Tr}\{s_\alpha G^R(\varepsilon+\hbar\omega_\Sigma)J_{\beta\gamma}[G^R(\varepsilon)-G^A(\varepsilon)] + s_\alpha[G^R(\varepsilon)-G^A(\varepsilon)]J_{\beta\gamma}G^A(\varepsilon-\hbar\omega_\Sigma)\}\\ &+ \mathrm{Tr}\{s_\alpha G^R(\varepsilon+\hbar\omega_\Sigma)J_\beta G^R(\varepsilon+\hbar\omega_2)J_\gamma[G^R(\varepsilon)-G^A(\varepsilon)] + s_\alpha G^R(\varepsilon+\hbar\omega_1)J_\beta[G^R(\varepsilon)\\ &- G^A(\varepsilon)]J_\gamma G^A(\varepsilon-\hbar\omega_2) + s_\alpha[G^R(\varepsilon)-G^A(\varepsilon)]J_\beta G^A(\varepsilon-\hbar\omega_1)J_\gamma G^A(\varepsilon-\hbar\omega_\Sigma)\}\Big) + [(\beta,\omega_1)\leftrightarrow(\gamma,\omega_2)],\end{aligned} \tag{A10}$$

where $\omega_\Sigma = \omega_1+\omega_2$. Lastly, using $\zeta^{(2)}_{\alpha;\beta\gamma}(\omega_\Sigma;\omega_1,\omega_2) = \chi^{(2)}_{\alpha;\beta\gamma}(\omega_\Sigma;\omega_1,\omega_2)/i(\omega_1+i\delta)i(\omega_2+i\delta)$ and changing the integration variable from ε to ω by $\varepsilon = \hbar\omega$, we can derive Eq. (10) in the main text.

APPENDIX B: DC LIMIT FOR THE RESPONSE FUNCTION

First, we expand the single-particle Green's function and the Fermi distribution function for small frequencies,

$$G^{R/A}(\omega+\omega_1) \simeq G^{R/A}(\omega) + \frac{\partial G^{R/A}(\omega)}{\partial\omega}\omega_1, \tag{B1}$$

$$G^{R/A}(\omega+\omega_1+\omega_2) \simeq G^{R/A}(\omega) + \frac{\partial G^{R/A}(\omega)}{\partial\omega}(\omega_1+\omega_2) + \frac{\partial^2 G^{R/A}(\omega)}{\partial\omega^2}\omega_1\omega_2, \tag{B2}$$

$$f(\omega+\omega_1) \simeq f(\omega) + \frac{\partial f(\omega)}{\partial\omega}\omega_1. \tag{B3}$$

Then, using these equations, we rewrite Eq. (10) as

$$\zeta^{(2)}_{\alpha;\beta\gamma}(\omega_1+\omega_2;\omega_1,\omega_2) = \frac{\hbar}{\omega_1\omega_2}\int_{-\infty}^{\infty}\frac{d\omega}{2\pi i}\left\{A_0(\omega) + A_1(\omega)\omega_1 + A_1'(\omega)\omega_2 + A_2(\omega)\omega_1\omega_2 + O\left(\omega_i^3\right)\right\}, \tag{B4}$$

where each component is given by

$$\begin{aligned} A_0(\omega) = \int \frac{d\boldsymbol{k}}{(2\pi)^d} f(\omega)\mathrm{Tr}\Big\{ &\frac{1}{2}[s_\alpha G^R(\omega)J_{\beta\gamma}G^R(\omega) - s_\alpha G^A(\omega)J_{\beta\gamma}G^A(\omega)] \\ &+ s_\alpha G^R(\omega)J_\beta G^R(\omega)J_\gamma G^R(\omega) - s_\alpha G^A(\omega)J_\beta G^A(\omega)J_\gamma G^A(\omega)\Big\} + (\beta \leftrightarrow \gamma), \end{aligned} \tag{B5}$$

$$\begin{aligned} A_1(\omega) = &\int \frac{d\boldsymbol{k}}{(2\pi)^d}\left(\frac{\partial f(\omega)}{\partial\omega}\right)\mathrm{Tr}[s_\alpha G^R(\omega)J_{\beta\gamma}G^A(\omega) + s_\alpha G^R(\omega)J_\beta G^A(\omega)J_\gamma G^A(\omega) + s_\alpha G^R(\omega)J_\gamma G^R(\omega)J_\beta G^A(\omega)] \\ &+ \int \frac{d\boldsymbol{k}}{(2\pi)^d} f(\omega)\Big\{\mathrm{Tr}\Big[s_\alpha\frac{\partial G^R(\omega)}{\partial\omega}J_{\beta\gamma}G^R(\omega) + s_\alpha\frac{\partial G^R(\omega)}{\partial\omega}J_\beta G^R(\omega)J_\gamma G^R(\omega) \\ &+ s_\alpha\frac{\partial G^R(\omega)}{\partial\omega}J_\gamma G^R(\omega)J_\beta G^R(\omega) + s_\alpha G^R(\omega)J_\gamma\frac{\partial G^R(\omega)}{\partial\omega}J_\beta G^R(\omega)\Big] + \text{c.c.}\Big\}, \end{aligned} \tag{B6}$$

$$A_1'(\omega) = A_1(\omega;\beta\leftrightarrow\gamma), \tag{B7}$$

$$\begin{aligned} A_2(\omega) = &\int \frac{d\boldsymbol{k}}{(2\pi)^d}\left(\frac{\partial f(\omega)}{\partial\omega}\right)\left\{\mathrm{Tr}\left[s_\alpha\frac{\partial G^R(\omega)}{\partial\omega}J_\beta G^R(\omega)J_\gamma G^A(\omega) + \frac{1}{2}s_\alpha\frac{\partial G^R(\omega)}{\partial\omega}J_{\beta\gamma}G^A(\omega)\right] - \text{c.c.}\right\} \\ &+ \int \frac{d\boldsymbol{k}}{(2\pi)^d} f(\omega)\left\{\mathrm{Tr}\left[s_\alpha\frac{\partial}{\partial\omega}\left(\frac{\partial G^R(\omega)}{\partial\omega}J_\beta G^R(\omega)\right)J_\gamma G^R(\omega) + \frac{1}{2}s_\alpha\frac{\partial^2 G^R(\omega)}{\partial\omega^2}J_{\beta\gamma}G^R(\omega)\right] - \text{c.c.}\right\} + (\beta\leftrightarrow\gamma). \end{aligned} \tag{B8}$$

Here, we use $(G^R)^\dagger = G^A$ when calculating the complex conjugates (c.c.). By using the following relation derived from the generalized Ward identity:

$$(q/\hbar)\partial_{k_\alpha}G^{R/A}(\boldsymbol{k},\omega) = G^{R/A}(\boldsymbol{k},\omega)J_\alpha(\boldsymbol{k})G^{R/A}(\boldsymbol{k},\omega), \tag{B9}$$

Eqs. (B5) and (B6) become

$$A_0(\omega) = \frac{q^2}{\hbar^2}\int\frac{d\boldsymbol{k}}{(2\pi)^d} f(\omega)\partial_{k_\gamma}\partial_{k_\beta}\mathrm{Tr}\{s_\alpha[G^R(\boldsymbol{k},\omega) - G^A(\boldsymbol{k},\omega)]\}, \tag{B10}$$

$$\begin{aligned} A_1(\omega) = \frac{q}{\hbar}\int\frac{d\boldsymbol{k}}{(2\pi)^d}\Bigg(&\left(\frac{\partial f(\omega)}{\partial\omega}\right)\partial_{k_\gamma}\mathrm{Tr}[s_\alpha G^R(\boldsymbol{k},\omega)J_\beta(\boldsymbol{k})G^A(\boldsymbol{k},\omega)] \\ &+ f(\omega)\left\{\partial_{k_\gamma}\mathrm{Tr}\left[s_\alpha\frac{\partial G^R(\boldsymbol{k},\omega)}{\partial\omega}J_\beta(\boldsymbol{k})G^R(\boldsymbol{k},\omega)\right] + \text{c.c.}\right\}\Bigg). \end{aligned} \tag{B11}$$

Equations (B10) and (B11) vanish because they are written as an integral over the corresponding derivative. Therefore, divergence does not occur even when we take the DC limit, and $A_2(\omega)$ determines the current-induced NEE.

APPENDIX C: BAND REPRESENTATION OF THE RESPONSE FUNCTION FOR THE DC LIMIT

In this section, we derive the band representation of the response function for the DC limit by taking the weak-scattering limit for Eq. (12). We define the Green's function of the nth band as

$$G_n^{R/A}(\boldsymbol{k},\omega)=\frac{1}{\hbar\omega-\varepsilon_n(\boldsymbol{k})\pm i\eta}, \tag{C1}$$

where η is a scattering rate. Here, we shift the integral variable ω and include the chemical potential μ into the Fermi distribution function: $f(\omega)=(1+e^{\beta(\hbar\omega-\mu)})^{-1}$. Note that weak scattering means that the scattering rate is sufficiently small compared to the kinetic energy of electrons, $1/\beta$, the energy of incident photons, $\hbar\omega_1$, and the interband energy, $\varepsilon_n-\varepsilon_m$. In the following, we first perform the frequency integral and then expand the resulting response function in powers of η to obtain the final expressions.

When we perform a partial integral in Eq. (12) and ignore the Fermi sea terms, Eq. (12) becomes

$$\begin{aligned}\zeta^{(2)}_{\alpha;\beta\gamma}=2\hbar\sum_{n,m,l}\int\frac{d\boldsymbol{k}}{(2\pi)^d}\int_{-\infty}^{\infty}\frac{d\omega}{2\pi}\Big(-\frac{\partial f(\omega)}{\partial\omega}\Big)\mathrm{Im}\Big[s^{nm}_{\alpha}(\boldsymbol{k})\frac{\partial G^R_m(\boldsymbol{k},\omega)}{\partial\omega}J^{ml}_{\beta}(\boldsymbol{k})G^R_l(\boldsymbol{k},\omega)J^{ln}_{\gamma}(\boldsymbol{k})G^{R-A}_n(\boldsymbol{k},\omega)\\+\frac{1}{2}s^{nm}_{\alpha}(\boldsymbol{k})\frac{\partial G^R_m(\boldsymbol{k},\omega)}{\partial\omega}J^{mn}_{\beta\gamma}(\boldsymbol{k})G^{R-A}_n(\boldsymbol{k},\omega)\Big]+(\beta\leftrightarrow\gamma).\end{aligned} \tag{C2}$$

Furthermore, we divide $\zeta^{(2)}_{\alpha;\beta\gamma}$ into

$$\zeta^{(2)}_{\alpha;\beta\gamma}=2\hbar^2q^2\int\frac{d\boldsymbol{k}}{(2\pi)^d}\big[\zeta^{(2),\mathrm{A}}_{\alpha;\beta\gamma}(\boldsymbol{k})+\zeta^{(2),\mathrm{B}}_{\alpha;\beta\gamma}(\boldsymbol{k})+\zeta^{(2),\mathrm{C}}_{\alpha;\beta\gamma}(\boldsymbol{k})+\zeta^{(2),\mathrm{D}}_{\alpha;\beta\gamma}(\boldsymbol{k})+\zeta^{(2),\mathrm{E}}_{\alpha;\beta\gamma}(\boldsymbol{k})\big]+(\beta\leftrightarrow\gamma), \tag{C3}$$

where each component is given by

$$\zeta^{(2),\mathrm{A}}_{\alpha;\beta\gamma}(\boldsymbol{k})=\frac{1}{2}\sum_{n}\int_{-\infty}^{\infty}\frac{d\omega}{2\pi}\Big(-\frac{\partial f(\omega)}{\hbar\partial\omega}\Big)\mathrm{Im}\Big[s^{nn}_{\alpha}\frac{\partial G^R_n(\omega)}{\partial\omega}v^{nn}_{\beta\gamma}G^{R-A}_n(\omega)\Big], \tag{C4}$$

$$\zeta^{(2),\mathrm{B}}_{\alpha;\beta\gamma}(\boldsymbol{k})=\sum_{n}\int_{-\infty}^{\infty}\frac{d\omega}{2\pi}\Big(-\frac{\partial f(\omega)}{\hbar\partial\omega}\Big)\mathrm{Im}\Big[s^{nn}_{\alpha}\frac{\partial G^R_n(\omega)}{\partial\omega}v^{nn}_{\beta}G^R_n(\omega)v^{nn}_{\gamma}G^{R-A}_n(\omega)\Big], \tag{C5}$$

$$\zeta^{(2),\mathrm{C}}_{\alpha;\beta\gamma}(\boldsymbol{k})=\sum_{\substack{n,m\\m\neq n}}\int_{-\infty}^{\infty}\frac{d\omega}{2\pi}\Big(-\frac{\partial f(\omega)}{\hbar\partial\omega}\Big)\mathrm{Im}\Big[s^{nn}_{\alpha}\frac{\partial G^R_n(\omega)}{\partial\omega}v^{nm}_{\beta}G^R_m(\omega)v^{mn}_{\gamma}G^{R-A}_n(\omega)\Big], \tag{C6}$$

$$\zeta^{(2),\mathrm{D}}_{\alpha;\beta\gamma}(\boldsymbol{k})=\sum_{\substack{n,m\\m\neq n}}\int_{-\infty}^{\infty}\frac{d\omega}{2\pi}\Big(-\frac{\partial f(\omega)}{\hbar\partial\omega}\Big)\mathrm{Im}\Big[s^{nm}_{\alpha}\frac{\partial G^R_m(\omega)}{\partial\omega}v^{mn}_{\beta}G^R_n(\omega)v^{nn}_{\gamma}G^{R-A}_n(\omega)\Big], \tag{C7}$$

$$\begin{aligned}\zeta^{(2),\mathrm{E}}_{\alpha;\beta\gamma}(\boldsymbol{k})=&\frac{1}{2}\sum_{\substack{n,m\\m\neq n}}\int_{-\infty}^{\infty}\frac{d\omega}{2\pi}\Big(-\frac{\partial f(\omega)}{\hbar\partial\omega}\Big)\mathrm{Im}\Big[s^{nm}_{\alpha}\frac{\partial G^R_m(\omega)}{\partial\omega}v^{mn}_{\beta\gamma}G^{R-A}_n(\omega)\Big]\\&+\sum_{\substack{n,m,l\\m\neq n,l\neq n}}\int_{-\infty}^{\infty}\frac{d\omega}{2\pi}\Big(-\frac{\partial f(\omega)}{\hbar\partial\omega}\Big)\mathrm{Im}\Big[s^{nm}_{\alpha}\frac{\partial G^R_m(\omega)}{\partial\omega}v^{ml}_{\beta}G^R_l(\omega)v^{ln}_{\gamma}G^{R-A}_n(\omega)\Big].\end{aligned} \tag{C8}$$

Here, $v_{\alpha_1\ldots\alpha_n}(\boldsymbol{k})=q^{-n}J_{\alpha_1\ldots\alpha_n}(\boldsymbol{k})$ is a velocity operator. When we perform a partial integral in $\zeta^{(2),\mathrm{B}}_{\alpha;\beta\gamma}(\boldsymbol{k})$, Eq. (C5) becomes

$$\zeta^{(2),\mathrm{B}}_{\alpha;\beta\gamma}(\boldsymbol{k})=\frac{1}{2}\sum_{n}\int_{-\infty}^{\infty}\frac{d\omega}{2\pi}\Big(\frac{\partial^2 f(\omega)}{\hbar\partial\omega^2}\Big)\mathrm{Im}\big[s^{nn}_{\alpha}G^R_n(\omega)v^{nn}_{\beta}G^R_n(\omega)v^{nn}_{\gamma}G^{R-A}_n(\omega)\big]. \tag{C9}$$

Assuming the weak-scattering limit yields

$$G^{R-A}_n(\omega)=\frac{-2i\eta}{(\hbar\omega-\varepsilon_n)^2+\eta^2}\sim-\frac{2\pi i}{\hbar}\delta(\omega-\varepsilon_n/\hbar), \tag{C10}$$

where $\delta(x)$ is the Dirac delta function. By performing the frequency integral using this equation, we find

$$\zeta^{(2),\mathrm{A}}_{\alpha;\beta\gamma}(\boldsymbol{k})=-\frac{1}{2\eta^2}\sum_{n}\mathrm{Re}\big(s^{nn}_{\alpha}v^{nn}_{\beta\gamma}\big)\Big(-\frac{\partial f_n}{\partial\varepsilon_n}\Big), \tag{C11}$$

$$\zeta^{(2),\mathrm{B}}_{\alpha;\beta\gamma}(\boldsymbol{k})=\frac{1}{2\eta^2}\sum_{n}\mathrm{Re}\big(s^{nn}_{\alpha}v^{nn}_{\beta}v^{nn}_{\gamma}\big)\Big(\frac{\partial^2 f_n}{\partial\varepsilon_n^2}\Big), \tag{C12}$$

$$\zeta^{(2),\mathrm{C}}_{\alpha;\beta\gamma}(\boldsymbol{k}) = -\frac{1}{\eta^2}\sum_{\substack{n,m\\ m\neq n}} \mathrm{Im}\left[i s^{nn}_{\alpha} \frac{v^{nm}_{\beta} v^{mn}_{\gamma}}{\varepsilon_{nm} + i\eta}\right]\left(-\frac{\partial f_n}{\partial \varepsilon_n}\right), \tag{C13}$$

$$\zeta^{(2),\mathrm{D}}_{\alpha;\beta\gamma}(\boldsymbol{k}) = \frac{1}{\eta}\sum_{\substack{n,m\\ m\neq n}} \mathrm{Im}\left[\frac{s^{nm}_{\alpha} v^{mn}_{\beta}}{(\varepsilon_{nm} + i\eta)^2} v^{nn}_{\gamma}\right]\left(-\frac{\partial f_n}{\partial \varepsilon_n}\right), \tag{C14}$$

$$\zeta^{(2),\mathrm{E}}_{\alpha;\beta\gamma}(\boldsymbol{k}) = \frac{1}{2}\sum_{\substack{n,m\\ m\neq n}} \mathrm{Im}\left[i \frac{s^{nm}_{\alpha} v^{mn}_{\beta\gamma}}{(\varepsilon_{nm} + i\eta)^2}\right]\left(-\frac{\partial f_n}{\partial \varepsilon_n}\right) + \sum_{\substack{n,m,l\\ m\neq n, l\neq n}} \mathrm{Im}\left[i \frac{s^{nm}_{\alpha} v^{ml}_{\beta} v^{ln}_{\gamma}}{(\varepsilon_{nm} + i\eta)^2(\varepsilon_{nl} + i\eta)}\right]\left(-\frac{\partial f_n}{\partial \varepsilon_n}\right), \tag{C15}$$

where $\varepsilon_{nm} = \varepsilon_n - \varepsilon_m$, and $f_n = f(\varepsilon_n) = (1 + e^{\beta(\varepsilon_n - \mu)})^{-1}$.

Then, expanding Eqs. (C13)–(C15) in powers of η up to the order of $O(\eta)$ results in

$$\begin{aligned}
\zeta^{(2),\mathrm{C}}_{\alpha;\beta\gamma}(\boldsymbol{k}) &= -\frac{1}{\eta^2}\sum_{\substack{n,m\\ m\neq n}} \mathrm{Im}\left[i s^{nn}_{\alpha} \frac{v^{nm}_{\beta} v^{mn}_{\gamma}}{\varepsilon^2_{nm} + \eta^2}(\varepsilon_{nm} - i\eta)\right]\left(-\frac{\partial f_n}{\partial \varepsilon_n}\right) \\
&= -\frac{1}{\eta^2}\sum_{\substack{n,m\\ m\neq n}} \mathrm{Im}\left[i s^{nn}_{\alpha} \frac{v^{nm}_{\beta} v^{mn}_{\gamma}}{\varepsilon_{nm}}\left(1 - \frac{\eta^2}{\varepsilon^2_{nm}}\right) + \eta s^{nn}_{\alpha} \frac{v^{nm}_{\beta} v^{mn}_{\gamma}}{\varepsilon^2_{nm}}\right]\left(-\frac{\partial f_n}{\partial \varepsilon_n}\right) + O(\eta) \\
&= \sum_{\substack{n,m\\ m\neq n}}\left\{ -\frac{1}{\eta^2}\mathrm{Re}\left[s^{nn}_{\alpha} \frac{v^{nm}_{\beta} v^{mn}_{\gamma}}{\varepsilon_{nm}}\right] + \mathrm{Re}\left[s^{nn}_{\alpha} \frac{v^{nm}_{\beta} v^{mn}_{\gamma}}{\varepsilon^3_{nm}}\right] - \frac{1}{\eta}\mathrm{Im}\left[s^{nn}_{\alpha} \frac{v^{nm}_{\beta} v^{mn}_{\gamma}}{\varepsilon^2_{nm}}\right]\right\}\left(-\frac{\partial f_n}{\partial \varepsilon_n}\right) + O(\eta),
\end{aligned} \tag{C16}$$

$$\begin{aligned}
\zeta^{(2),\mathrm{D}}_{\alpha;\beta\gamma}(\boldsymbol{k}) &= \frac{1}{\eta}\sum_{\substack{n,m\\ m\neq n}} \mathrm{Im}\left[\frac{s^{nm}_{\alpha} v^{mn}_{\beta}}{\left(\varepsilon^2_{nm} + \eta^2\right)^2} v^{nn}_{\gamma}(\varepsilon_{nm} - i\eta)^2\right]\left(-\frac{\partial f_n}{\partial \varepsilon_n}\right) \\
&= \sum_{\substack{n,m\\ m\neq n}}\left\{ \frac{1}{\eta}\mathrm{Im}\left[\frac{s^{nm}_{\alpha} v^{mn}_{\beta}}{\varepsilon^2_{nm}} v^{nn}_{\gamma}\right] - 2\mathrm{Re}\left[\frac{s^{nm}_{\alpha} v^{mn}_{\beta}}{\varepsilon^3_{nm}} v^{nn}_{\gamma}\right]\right\}\left(-\frac{\partial f_n}{\partial \varepsilon_n}\right) + O(\eta),
\end{aligned} \tag{C17}$$

$$\begin{aligned}
\zeta^{(2),\mathrm{E}}_{\alpha;\beta\gamma}(\boldsymbol{k}) &= \frac{1}{2}\sum_{\substack{n,m\\ m\neq n}} \mathrm{Im}\left[i \frac{s^{nm}_{\alpha} v^{mn}_{\beta\gamma}}{\left(\varepsilon^2_{nm} + \eta^2\right)^2}(\varepsilon_{nm} - i\eta)^2\right]\left(-\frac{\partial f_n}{\partial \varepsilon_n}\right) \\
&\quad + \sum_{\substack{n,m,l\\ m\neq n, l\neq n}} \mathrm{Im}\left[i \frac{s^{nm}_{\alpha} v^{ml}_{\beta} v^{ln}_{\gamma}}{\left(\varepsilon^2_{nm} + \eta^2\right)^2\left(\varepsilon^2_{nl} + \eta^2\right)}(\varepsilon_{nm} - i\eta)^2(\varepsilon_{nl} - i\eta)\right]\left(-\frac{\partial f_n}{\partial \varepsilon_n}\right) \\
&= \frac{1}{2}\sum_{\substack{n,m\\ m\neq n}} \mathrm{Re}\left[\frac{s^{nm}_{\alpha} v^{mn}_{\beta\gamma}}{\varepsilon^2_{nm}}\right]\left(-\frac{\partial f_n}{\partial \varepsilon_n}\right) + \sum_{\substack{n,m,l\\ m\neq n, l\neq n}} \mathrm{Re}\left[\frac{s^{nm}_{\alpha} v^{ml}_{\beta} v^{ln}_{\gamma}}{\varepsilon^2_{nm}\varepsilon_{nl}}\right]\left(-\frac{\partial f_n}{\partial \varepsilon_n}\right) + O(\eta).
\end{aligned} \tag{C18}$$

Replacing η with $\hbar/\tau$, where τ is a relaxation time, and classifying $\zeta^{(2)}_{\alpha;\beta\gamma}$ according to powers of τ, we obtain

$$\begin{aligned}
\zeta^{(2),\tau^2}_{\alpha;\beta\gamma} &= q^2\tau^2 \sum_n \int \frac{d\boldsymbol{k}}{(2\pi)^d} \mathrm{Re}\left[s^{nn}_{\alpha} v^{nn}_{\beta} v^{nn}_{\gamma}\left(\frac{\partial^2 f_n}{\partial \varepsilon^2_n}\right) + \left(s^{nn}_{\alpha} v^{nn}_{\beta\gamma} + 2\sum_{m(\neq n)} s^{nn}_{\alpha} \frac{v^{nm}_{\beta} v^{mn}_{\gamma}}{\varepsilon_{nm}}\right)\left(\frac{\partial f_n}{\partial \varepsilon_n}\right)\right] + (\beta \leftrightarrow \gamma) \\
&= \frac{2q^2}{\hbar^2}\tau^2 \sum_n \int \frac{d\boldsymbol{k}}{(2\pi)^d} s^{nn}_{\alpha} \partial_{k_\beta}\partial_{k_\gamma} f_n,
\end{aligned} \tag{C19}$$

$$\begin{aligned}
\zeta^{(2),\tau}_{\alpha;\beta\gamma} &= 2\hbar q^2\tau \sum_{\substack{n,m\\ m\neq n}} \int \frac{d\boldsymbol{k}}{(2\pi)^d} \mathrm{Im}\left[\frac{s^{nm}_{\alpha} v^{mn}_{\beta}}{\varepsilon^2_{nm}} v^{nn}_{\gamma}\right]\left(-\frac{\partial f_n}{\partial \varepsilon_n}\right) - 2\hbar q^2\tau \sum_{\substack{n,m\\ m\neq n}} \int \frac{d\boldsymbol{k}}{(2\pi)^d} \mathrm{Im}\left[s^{nn}_{\alpha} \frac{v^{nm}_{\beta} v^{mn}_{\gamma}}{\varepsilon^2_{nm}}\right]\left(-\frac{\partial f_n}{\partial \varepsilon_n}\right) + (\beta \leftrightarrow \gamma) \\
&= -q^2\tau \sum_{\substack{n,m\\ m\neq n}} \int \frac{d\boldsymbol{k}}{(2\pi)^d} 2\mathrm{Im}\left[\frac{s^{nm}_{\alpha} v^{mn}_{\beta}}{\varepsilon^2_{nm}}\right]\partial_{k_\gamma} f_n + (\beta \leftrightarrow \gamma),
\end{aligned} \tag{C20}$$

$$\zeta^{(2),\tau^0}_{\alpha;\beta\gamma} = \hbar^2 q^2 \sum_{\substack{n,m \\ m\neq n}} \int \frac{d\boldsymbol{k}}{(2\pi)^d} \mathrm{Re}\left[\frac{s^{nm}_\alpha}{\varepsilon^2_{nm}}\left(v^{mn}_{\beta\gamma} + \sum_{l(\neq n)} 2\frac{v^{ml}_\beta v^{ln}_\gamma}{\varepsilon_{nl}}\right) + 2s^{nn}_\alpha \frac{v^{nm}_\beta v^{mn}_\gamma}{\varepsilon^3_{nm}} - 4\frac{s^{nm}_\alpha v^{mn}_\beta}{\varepsilon^3_{nm}} v^{nn}_\gamma\right]\left(-\frac{\partial f_n}{\partial \varepsilon_n}\right) + (\beta \leftrightarrow \gamma), \tag{C21}$$

where $\zeta^{(2),\tau^n}_{\alpha;\beta\gamma} = O(\tau^n)$, and we use

$$\hbar^{-1}\partial_{k_\beta} v^{nn}_\gamma = v^{nn}_{\beta\gamma} + \sum_{m(\neq n)} \frac{v^{nm}_\beta v^{mn}_\gamma + v^{nm}_\gamma v^{mn}_\beta}{\varepsilon_{nm}}, \tag{C22}$$

to derive Eq. (C19), and drop the second term in the first line of Eq. (C20) because it cancels out with the corresponding term where the indices of the electric fields are interchanged. The τ^2 term and τ term are consistent with Eq. (68) of Ref. [48] and Eq. (6) of Ref. [42], respectively. As for the τ^0 term, the second and third terms of Eq. (C21) are consistent with the Fermi surface terms of Eq. (9) in Ref. [53].

APPENDIX D: BAND REPRESENTATION OF THE RESPONSE FUNCTION FOR FINITE FREQUENCIES

In this section, we derive the band representation of the response function for finite frequencies by taking the weak-scattering limit. In the following, we first derive the spin density using the RDM formalism in the velocity gauge and then compare it with the result of taking the weak-scattering limit for Eq. (10). Note that the RDM formalism in the length gauge was derived in Ref. [48].

1. Reduced density matrix formalism in the velocity gauge

Instead of the full density matrix $\hat{\rho}(t)$, we only have to consider the dynamics of the RDM $\hat{\rho}_{\boldsymbol{k}}(t)$ in a subspace $\mathbb{V}_{\boldsymbol{k}}$ labeled by crystal momentum $\boldsymbol{k}$. This is because we can express $\hat{\rho}(t)$ as a tensor product of the RDMs: $\hat{\rho}(t) = \prod_{\boldsymbol{k}} \otimes \hat{\rho}_{\boldsymbol{k}}(t)$, and we first solve the equation of motion for the RDM. The matrix representation of the RDM is

$$\rho_{\boldsymbol{k}nm}(t) = \mathrm{Tr}[\hat{\rho}(t)\hat{c}^\dagger_{\boldsymbol{k}m}\hat{c}_{\boldsymbol{k}n}], \tag{D1}$$

where $\hat{c}^\dagger_{\boldsymbol{k}n}$ and $\hat{c}_{\boldsymbol{k}n}$ are fermionic creation and annihilation operators with the momentum $\boldsymbol{k}$ and a band n. According to the von Neumann equation, $i\hbar\partial_t\hat{\rho}(t) = [\hat{H}(t), \hat{\rho}(t)]$, the equation of motion for the RDM is described as

$$i\hbar\partial_t \rho_{\boldsymbol{k}nm}(t) = \mathrm{Tr}\{\hat{\rho}(t)[\hat{c}^\dagger_{\boldsymbol{k}m}\hat{c}_{\boldsymbol{k}n}, \hat{H}(t)]\}, \tag{D2}$$

where $\partial_t = \partial/\partial t$, $\hat{H}(t)$ is a general Hamiltonian and the inner bracket denotes the commutator. Here, we assume $\hat{H}(t) = \hat{H}_0 + \hat{V}(t)$, where $\hat{H}_0$ is an unperturbed Hamiltonian and $\hat{V}(t)$ is a perturbation by an external field $\boldsymbol{F}(t)$. These Hamiltonians are described as

$$\hat{H}_0 = \sum_n \int \frac{d\boldsymbol{k}}{(2\pi)^d} \varepsilon_{\boldsymbol{k}n}\hat{c}^\dagger_{\boldsymbol{k}n}\hat{c}_{\boldsymbol{k}n}, \quad \hat{V}(t) = \sum_{n,m}\int \frac{d\boldsymbol{k}}{(2\pi)^d}\hat{c}^\dagger_{\boldsymbol{k}n}V_{\boldsymbol{k}nm}(t)\hat{c}_{\boldsymbol{k}m}. \tag{D3}$$

By using anticommutation relations,

$$\{\hat{c}_{\boldsymbol{k}n}, \hat{c}_{\boldsymbol{k}'m}\} = \{\hat{c}^\dagger_{\boldsymbol{k}n}, \hat{c}^\dagger_{\boldsymbol{k}'m}\} = 0, \quad \{\hat{c}_{\boldsymbol{k}n}, \hat{c}^\dagger_{\boldsymbol{k}'m}\} = (2\pi)^d\delta_{nm}\delta(\boldsymbol{k}-\boldsymbol{k}'), \tag{D4}$$

Eq. (D2) becomes

$$(i\hbar\partial_t - \varepsilon_{\boldsymbol{k}nm})\rho_{\boldsymbol{k}nm}(t) = [V_{\boldsymbol{k}}(t), \rho_{\boldsymbol{k}}(t)]_{nm}, \tag{D5}$$

where $\varepsilon_{\boldsymbol{k}nm} = \varepsilon_{\boldsymbol{k}n} - \varepsilon_{\boldsymbol{k}m}$, and $[V_{\boldsymbol{k}}(t), \rho_{\boldsymbol{k}}(t)]_{nm} = \sum_l [V_{\boldsymbol{k}nl}(t)\rho_{\boldsymbol{k}lm}(t) - \rho_{\boldsymbol{k}nl}(t)V_{\boldsymbol{k}lm}(t)]$. Here, we present a phenomenological treatment of the scattering rate [80]. The scattering rate η is introduced by modifying Eq. (D5) to

$$(i\hbar\partial_t - \varepsilon_{\boldsymbol{k}nm})\rho^{(p)}_{\boldsymbol{k}nm}(t) = \sum_{q=0}^{p}\left[V^{(p-q)}_{\boldsymbol{k}}(t), \rho^{(q)}_{\boldsymbol{k}}(t)\right]_{nm} - ip\eta\rho^{(p)}_{\boldsymbol{k}nm}(t), \tag{D6}$$

where we focus on the equation for the pth-order RDM, $\rho^{(p)}_{\boldsymbol{k}nm}(t)$, by expanding $\rho_{\boldsymbol{k}nm}(t)$ and $V_{\boldsymbol{k}nm}(t)$ in powers of $\boldsymbol{F}(t)$: $\rho_{\boldsymbol{k}nm}(t) = \sum_p \rho^{(p)}_{\boldsymbol{k}nm}(t)$ and $V_{\boldsymbol{k}nm}(t) = \sum_p V^{(p)}_{\boldsymbol{k}nm}(t)$ with $\rho^{(p)}_{\boldsymbol{k}nm}, V^{(p)}_{\boldsymbol{k}nm} = O(|\boldsymbol{F}|^p)$. Furthermore, taking the Fourier transformation results in

$$(\hbar\omega - \varepsilon_{\boldsymbol{k}nm} + ip\eta)\rho^{(p)}_{\boldsymbol{k}nm}(\omega) = \int \frac{d\omega_1}{2\pi}\frac{d\omega_2}{2\pi}\sum_{q=0}^{p}\left[V^{(p-q)}_{\boldsymbol{k}}(\omega_1), \rho^{(q)}_{\boldsymbol{k}}(\omega_2)\right]_{nm} 2\pi\,\delta_{\omega_1+\omega_2,\omega}. \tag{D7}$$

Then, we derive the pth-order RDM, $\rho^{(p)}_{\boldsymbol{k}nm}(\omega)$, in the velocity gauge and calculate the expectation value of the spin density. From Eq. (5), we can express $\hat{H}(t)$ as

$$\hat{H}(t) = \hat{H}_0\left[\boldsymbol{k} - \frac{q}{\hbar}\boldsymbol{A}(t)\right] = \hat{H}_0(\boldsymbol{k}) - q\hat{v}_\beta(\boldsymbol{k})A^\beta(t) + \frac{q^2}{2}\hat{v}_{\beta\gamma}(\boldsymbol{k})A^\beta(t)A^\gamma(t) + \cdots, \tag{D8}$$

where $\hat{v}_{\alpha_1\ldots\alpha_n}(\boldsymbol{k}) = (1/\hbar)^n\partial_{k_{\alpha_1}}\ldots\partial_{k_{\alpha_n}}\hat{H}_0(\boldsymbol{k})$ is a velocity operator. When we perform the Fourier transformation, $V^{(p)}_{\boldsymbol{k}nm}(\omega)$ ($p = 1, 2$) are given by

$$V^{(1)}_{\boldsymbol{k}nm}(\omega) = -qv^{nm}_\beta\int\frac{d\omega_1}{2\pi}A^\beta(\omega_1)2\pi\delta_{\omega_1,\omega}, \tag{D9}$$

$$V^{(2)}_{\boldsymbol{k}nm}(\omega) = \frac{q^2}{2}v^{nm}_{\beta\gamma}\int\frac{d\omega_1}{2\pi}\frac{d\omega_2}{2\pi}A^\beta(\omega_1)A^\gamma(\omega_2)2\pi\delta_{\omega_1+\omega_2,\omega}. \tag{D10}$$

Thus, the pth-order RDMs ($p = 0, 1, 2$) are expressed as $\rho^{(0)}_{\boldsymbol{k}nm}(\omega) := \delta_{nm}f_m2\pi\delta(\omega)$ with the Fermi distribution function f_m, and

$$\rho^{(1)}_{\boldsymbol{k}nm}(\omega) = \int\frac{d\omega_1}{2\pi}\frac{qv^{nm}_\beta f_{nm}}{\hbar\omega_1 - \varepsilon_{nm} + i\eta}A^\beta(\omega_1)2\pi\delta_{\omega_1,\omega}, \tag{D11}$$

$$\begin{aligned}\rho^{(2)}_{\boldsymbol{k}nm}(\omega) = {}& \int\frac{d\omega_1}{2\pi}\frac{d\omega_2}{2\pi}A^\beta(\omega_1)A^\gamma(\omega_2)2\pi\delta_{\omega_1+\omega_2,\omega}\\ &\times q^2\left[\frac{1}{2}\frac{v^{nm}_{\beta\gamma}f_{mn}}{\hbar\omega - \varepsilon_{nm} + 2i\eta} + \sum_l\frac{1}{\hbar\omega - \varepsilon_{nm} + 2i\eta}\left(\frac{v^{nl}_\beta v^{lm}_\gamma f_{ml}}{\hbar\omega_2 - \varepsilon_{lm} + i\eta} - \frac{v^{nl}_\gamma v^{lm}_\beta f_{ln}}{\hbar\omega_2 - \varepsilon_{nl} + i\eta}\right)\right],\end{aligned} \tag{D12}$$

where $f_{nm} = f_n - f_m$. The expectation value of the spin density is calculated by using the spin operator and the RDM,

$$\langle\delta\hat{s}_\alpha(\omega)\rangle = \sum_{n,m}\int\frac{d\boldsymbol{k}}{(2\pi)^d}s^{nm}_\alpha(\boldsymbol{k})\rho_{\boldsymbol{k}mn}(\omega). \tag{D13}$$

In particular, the second-order spin density $\langle\delta\hat{s}_\alpha(\omega)\rangle^{(2)}$ with respect to the electric field is given by

$$\begin{aligned}\langle\delta\hat{s}_\alpha(\omega)\rangle^{(2)} = {}& 2\sum_{n,m}\int\frac{d\boldsymbol{k}}{(2\pi)^d}s^{nm}_\alpha\rho^{(2)}_{\boldsymbol{k}mn}(\omega)\\ = {}& \int\frac{d\omega_1}{2\pi}\frac{d\omega_2}{2\pi}E^\beta(\omega_1)E^\gamma(\omega_2)2\pi\delta_{\omega_1+\omega_2,\omega}\\ &\times -\frac{q^2}{(\omega_1 + i\delta)(\omega_2 + i\delta)}\sum_{n,m}\int\frac{d\boldsymbol{k}}{(2\pi)^d}\left[\frac{1}{2}\frac{s^{nm}_\alpha v^{mn}_{\beta\gamma}f_{nm}}{\hbar\omega - \varepsilon_{mn} + 2i\eta}\right.\\ &\left.+\sum_l\frac{s^{nm}_\alpha}{\hbar\omega - \varepsilon_{mn} + 2i\eta}\left(\frac{v^{ml}_\beta v^{ln}_\gamma f_{nl}}{\hbar\omega_2 - \varepsilon_{ln} + i\eta} - \frac{v^{ml}_\gamma v^{ln}_\beta f_{lm}}{\hbar\omega_2 - \varepsilon_{ml} + i\eta}\right)\right] + [(\beta,\omega_1)\leftrightarrow(\gamma,\omega_2)].\end{aligned} \tag{D14}$$

Here, we multiply a factor of 2 in the first line of the above expression to include the term interchanging the indices and frequencies of the electric fields. This additional contribution is reflected in the term $[(\beta,\omega_1)\leftrightarrow(\gamma,\omega_2)]$. Furthermore, we replace the vector potentials $\boldsymbol{A}(\omega_j)$ with electric fields $\boldsymbol{E}(\omega_j)$ by using $\boldsymbol{E}(\omega_j) = i(\omega_j + i\delta)\boldsymbol{A}(\omega_j)$.

2. Weak-scattering limit for Eq. (10)

Considering Eqs. (C1) and (C10), we can describe Eq. (10) as

$$\begin{aligned}\zeta^{(2)}_{\alpha;\beta\gamma}(\omega;\omega_1,\omega_2) = {}& -\frac{q^2}{(\omega_1 + i\delta)(\omega_2 + i\delta)}\sum_{n,m}\int\frac{d\boldsymbol{k}}{(2\pi)^d}\left\{\frac{1}{2}\frac{s^{nm}_\alpha v^{mn}_{\beta\gamma}f_{nm}}{\hbar\omega - \varepsilon_{mn} + i\eta}\right.\\ &+\sum_l\frac{s^{nm}_\alpha v^{ml}_\beta v^{ln}_\gamma}{(\hbar\omega - \varepsilon_{mn} + i\eta)(\hbar\omega_1 - \varepsilon_{ml} + i\eta)(\hbar\omega_2 - \varepsilon_{ln} + i\eta)}\\ &\left.\times[(\hbar\omega_1 - \varepsilon_{ml} + i\eta)f_n - (\hbar\omega - \varepsilon_{mn} + i\eta)f_l + (\hbar\omega_2 - \varepsilon_{ln} + i\eta)f_m]\right\} + [(\beta,\omega_1)\leftrightarrow(\gamma,\omega_2)],\end{aligned} \tag{D15}$$

where we change ω_Σ with ω after the calculation. Then, we replace $\hbar\omega + i\eta$ with $\hbar\omega + 2i\eta$ for a technical reason. Note that this modification has an impact on the results in the region of a peak ($\hbar\omega = \varepsilon_{nm}$) and in the low-frequency region for the diagonal response ($n = m$), as already pointed out in Refs. [55,81]. Using this modification, we find

$$\zeta^{(2)}_{\alpha;\beta\gamma}(\omega;\omega_1,\omega_2) = -\frac{q^2}{(\omega_1+i\delta)(\omega_2+i\delta)}\sum_{n,m}\int\frac{d\boldsymbol{k}}{(2\pi)^d}\Bigg[\frac{1}{2}\frac{s^{nm}_\alpha v^{mn}_{\beta\gamma} f_{nm}}{\hbar\omega-\varepsilon_{mn}+2i\eta} + \sum_l \frac{s^{nm}_\alpha}{\hbar\omega-\varepsilon_{mn}+2i\eta}\left(\frac{v^{ml}_\beta v^{ln}_\gamma f_{nl}}{\hbar\omega_2-\varepsilon_{ln}+i\eta} - \frac{v^{ml}_\gamma v^{ln}_\beta f_{lm}}{\hbar\omega_2-\varepsilon_{ml}+i\eta}\right)\Bigg] + [(\beta,\omega_1)\leftrightarrow(\gamma,\omega_2)], \tag{D16}$$

which is consistent with Eq. (D14).

[1] I. Žutić, J. Fabian, and S. D. Sarma, Spintronics: Fundamentals and applications, Rev. Mod. Phys. **76**, 323 (2004).

[2] S. D. Bader and S. S. P. Parkin, Spintronics, Annu. Rev. Condens. Matter Phys. **1**, 71 (2010).

[3] A. Hirohata, K. Yamada, Y. Nakatani, I.-L. Prejbeanu, B. Diény, P. Pirro, and B. Hillebrands, Review on spintronics: Principles and device applications, J. Magn. Magn. Mater. **509**, 166711 (2020).

[4] A. G. Aronov and Yu. B. Lyanda-Geller, Nuclear electric resonance and orientation of carrier spins by an electric field, JETP Lett. **50**, 431 (1989).

[5] V. M. Edelstein, Spin polarization of conduction electrons induced by electric current in two-dimensional asymmetric electron systems, Solid State Commun. **73**, 233 (1990).

[6] Y. K. Kato, R. C. Myers, A. C. Gossard, and D. D. Awschalom, Current-induced spin polarization in strained semiconductors, Phys. Rev. Lett. **93**, 176601 (2004).

[7] A. Y. Silov, P. A. Blajnov, J. H. Wolter, R. Hey, K. H. Ploog, and N. S. Averkiev, Current-induced spin polarization at a single heterojunction, Appl. Phys. Lett. **85**, 5929 (2004).

[8] S. D. Ganichev, S. N. Danilov, P. Schneider, V. V. Bel'kov, L. E. Golub, W. Wegscheider, D. Weiss, and W. Prettl, Electric current-induced spin orientation in quantum well structures, J. Magn. Magn. Mater. **300**, 127 (2006).

[9] A. Manchon and S. Zhang, Theory of nonequilibrium intrinsic spin torque in a single nanomagnet, Phys. Rev. B **78**, 212405 (2008).

[10] A. Manchon and S. Zhang, Theory of spin torque due to spin-orbit coupling, Phys. Rev. B **79**, 094422 (2009).

[11] I. Garate and A. H. MacDonald, Influence of a transport current on magnetic anisotropy in gyrotropic ferromagnets, Phys. Rev. B **80**, 134403 (2009).

[12] A. Chernyshov, M. Overby, X. Liu, J. K. Furdyna, Y. Lyanda-Geller, and L. P. Rokhinson, Evidence for reversible control of magnetization in a ferromagnetic material by means of spin–orbit magnetic field, Nat. Phys. **5**, 656 (2009).

[13] D. Pesin and A. H. MacDonald, Spintronics and pseudospintronics in graphene and topological insulators, Nat. Mater. **11**, 409 (2012).

[14] A. R. Mellnik, J. S. Lee, A. Richardella, J. L. Grab, P. J. Mintun, M. H. Fischer, A. Vaezi, A. Manchon, E.-A. Kim, N. Samarth, and D. C. Ralph, Spin-transfer torque generated by a topological insulator, Nature (London) **511**, 449 (2014).

[15] Y. Ando, T. Hamasaki, T. Kurokawa, K. Ichiba, F. Yang, M. Novak, S. Sasaki, K. Segawa, Y. Ando, and M. Shiraishi, Electrical detection of the spin polarization due to charge flow in the surface state of the topological insulator $Bi_{1.5}Sb_{0.5}Te_{1.7}Se_{1.3}$, Nano Lett. **14**, 6226 (2014).

[16] C. H. Li, O. M. J. van 't Erve, J. T. Robinson, Y. Liu, L. Li, and B. T. Jonker, Electrical detection of charge-current-induced spin polarization due to spin-momentum locking in Bi_2Se_3, Nat. Nanotechnol. **9**, 218 (2014).

[17] M. Rodriguez-Vega, G. Schwiete, J. Sinova, and E. Rossi, Giant Edelstein effect in topological-insulator–graphene heterostructures, Phys. Rev. B **96**, 235419 (2017).

[18] J. H. Cullen, R. B. Atencia, and D. Culcer, Spin transfer torques due to the bulk states of topological insulators, Nanoscale **15**, 8437 (2023).

[19] A. Johansson, J. Henk, and I. Mertig, Edelstein effect in Weyl semimetals, Phys. Rev. B **97**, 085417 (2018).

[20] B. Zhao, B. Karpiak, D. Khokhriakov, A. Johansson, A. M. Hoque, X. Xu, Y. Jiang, I. Mertig, and S. P. Dash, Unconventional charge-spin conversion in Weyl-semimetal WTe_2, Adv. Mater. **32**, 2000818 (2020).

[21] K. Limtragool and K. Pasanai, Large enhancement of Edelstein effect in Weyl semimetals from Fermi-arc surface states, Physica E **135**, 114983 (2022).

[22] A. A. Burkov, M. Smith, A. Hickey, and I. Martin, Current-induced spin accumulation and magnetoresistance in chiral semimetals, Phys. Rev. B **108**, 205115 (2023).

[23] V. M. Edelstein, Magnetoelectric effect in polar superconductors, Phys. Rev. Lett. **75**, 2004 (1995).

[24] W.-Y. He and K. T. Law, Magnetoelectric effects in gyrotropic superconductors, Phys. Rev. Res. **2**, 012073(R) (2020).

[25] Y. Ikeda and Y. Yanase, Giant surface Edelstein effect in d-wave superconductors, Phys. Rev. B **102**, 214510 (2020).

[26] R. Nakajima, D. Hirobe, G. Kawaguchi, Y. Nabei, T. Sato, T. Narushima, H. Okamoto, and H. M. Yamamoto, Giant spin polarization and a pair of antiparallel spins in a chiral superconductor, Nature (London) **613**, 479 (2023).

[27] K. Shinada and R. Peters, Unique properties of the optical activity in noncentrosymmetric superconductors: Sum rule, missing area, and relation with the superconducting Edelstein effect, Phys. Rev. B **108**, 165119 (2023).

[28] N. F. Q. Yuan, Edelstein effect and supercurrent diode effect, arXiv:2311.11087.

[29] S. Fujimoto, Fermi liquid theory for heavy fermion superconductors without inversion symmetry: Magnetism and transport coefficients, J. Phys. Soc. Jpn. **76**, 034712 (2007).

[30] S. Fujimoto, Electron correlation and pairing states in superconductors without inversion symmetry, J. Phys. Soc. Jpn. **76**, 051008 (2007).

[31] Y. Yanase, Magneto-electric effect in three-dimensional coupled zigzag chains, J. Phys. Soc. Jpn. **83**, 014703 (2014).

[32] R. Peters and Y. Yanase, Strong enhancement of the Edelstein effect in f-electron systems, Phys. Rev. B **97**, 115128 (2018).

[33] Y. Michishita and R. Peters, Effects of renormalization and non-Hermiticity on nonlinear responses in strongly correlated electron systems, Phys. Rev. B **103**, 195133 (2021).

[34] Y. Murakami, M. Eckstein, and P. Werner, High-harmonic generation in Mott insulators, Phys. Rev. Lett. **121**, 057405 (2018).

[35] N. Tancogne-Dejean, M. A. Sentef, and A. Rubio, Ultrafast modification of Hubbard u in a strongly correlated material: *Ab initio* high-harmonic generation in NiO, Phys. Rev. Lett. **121**, 097402 (2018).

[36] A. Kofuji, Y. Michishita, and R. Peters, Effects of strong correlations on the nonlinear response in Weyl-Kondo semimetals, Phys. Rev. B **104**, 085151 (2021).

[37] H. Kishida, H. Matsuzaki, H. Okamoto, T. Manabe, M. Yamashita, Y. Taguchi, and Y. Tokura, Gigantic optical nonlinearity in one-dimensional Mott-Hubbard insulators, Nature (London) **405**, 929 (2000).

[38] H. Liu, Y. Li, Y. S. You, S. Ghimire, T. F. Heinz, and D. A. Reis, High-harmonic generation from an atomically thin semiconductor, Nat. Phys. **13**, 262 (2017).

[39] S. Dzsaber, X. Yan, M. Taupin, G. Eguchi, A. Prokofiev, T. Shiroka, P. Blaha, O. Rubel, S. E. Grefe, H.-H. Lai, Q. Si, and S. Paschen, Giant spontaneous Hall effect in a nonmagnetic Weyl-Kondo semimetal, Proc. Natl. Acad. Sci. USA **118**, e2013386118 (2021).

[40] K. Uchida, G. Mattoni, S. Yonezawa, F. Nakamura, Y. Maeno, and K. Tanaka, High-order harmonic generation and its unconventional scaling law in the Mott-insulating Ca_2RuO_4, Phys. Rev. Lett. **128**, 127401 (2022).

[41] Y. Murakami, K. Uchida, A. Koga, K. Tanaka, and P. Werner, Anomalous temperature dependence of high-harmonic generation in Mott insulators, Phys. Rev. Lett. **129**, 157401 (2022).

[42] C. Xiao, W. Wu, H. Wang, Y.-X. Huang, X. Feng, H. Liu, G.-Y. Guo, Q. Niu, and S. A. Yang, Time-reversal-even nonlinear current induced spin polarization, Phys. Rev. Lett. **130**, 166302 (2023).

[43] I. Baek, S. Han, S. Cheon, and H.-W. Lee, Nonlinear orbital and spin Edelstein effect in centrosymmetric metals, npj Spintronics **2**, 33 (2024).

[44] R. Guo, Y.-X. Huang, X. Yang, Y. Liu, C. Xiao, and Z. Yuan, Extrinsic contribution to nonlinear current induced spin polarization, Phys. Rev. B **109**, 235413 (2024).

[45] M. Battiato, G. Barbalinardo, and P. M. Oppeneer, Quantum theory of the inverse Faraday effect, Phys. Rev. B **89**, 014413 (2014).

[46] M. Berritta, R. Mondal, K. Carva, and P. M. Oppeneer, *Ab initio* theory of coherent laser-induced magnetization in metals, Phys. Rev. Lett. **117**, 137203 (2016).

[47] H. Xu, J. Zhou, H. Wang, and J. Li, Light-induced static magnetization: Nonlinear Edelstein effect, Phys. Rev. B **103**, 205417 (2021).

[48] B. M. Fregoso, Bulk photospin effect: Calculation of electric spin susceptibility to second order in an electric field, Phys. Rev. B **106**, 195108 (2022).

[49] W. T. H. Koch, R. Munser, W. Ruppel, and P. Würfel, Anomalous photovoltage in $BaTiO_3$, Ferroelectrics **13**, 305 (1976).

[50] R. von Baltz and W. Kraut, Theory of the bulk photovoltaic effect in pure crystals, Phys. Rev. B **23**, 5590 (1981).

[51] Z. Dai and A. M. Rappe, Recent progress in the theory of bulk photovoltaic effect, Chem. Phys. Rev. **4**, 011303 (2023).

[52] P. Curie, On symmetry in physical phenomena, symmetry of an electric field and a magnetic field, J. Phys. Theor. Appl. **3**, 393 (1894).

[53] C. Xiao, H. Liu, W. Wu, H. Wang, Q. Niu, and S. A. Yang, Intrinsic nonlinear electric spin generation in centrosymmetric magnets, Phys. Rev. Lett. **129**, 086602 (2022).

[54] X. Feng, W. Wu, H. Wang, W. Gao, L. K. Ang, Y. X. Zhao, C. Xiao, and S. A. Yang, Quantum metric nonlinear spin-orbit torque enhanced by topological bands, arXiv:2402.00532.

[55] D. E. Parker, T. Morimoto, J. Orenstein, and J. E. Moore, Diagrammatic approach to nonlinear optical response with application to Weyl semimetals, Phys. Rev. B **99**, 045121 (2019).

[56] S. M. João and J. Viana Parente Lopes, Basis-independent spectral methods for non-linear optical response in arbitrary tight-binding models, J. Phys.: Condens. Matter **32**, 125901 (2020).

[57] Z. Z. Du, C. M. Wang, H.-P. Sun, H.-Z. Lu, and X. C. Xie, Quantum theory of the nonlinear Hall effect, Nat. Commun. **12**, 5038 (2021).

[58] Y. D. Wang, Z.-G. Zhu, and G. Su, Quantum theory of nonlinear thermal response, Phys. Rev. B **106**, 035148 (2022).

[59] A. Georges, G. Kotliar, W. Krauth, and M. J. Rozenberg, Dynamical mean-field theory of strongly correlated fermion systems and the limit of infinite dimensions, Rev. Mod. Phys. **68**, 13 (1996).

[60] M. Oestreich, M. Bender, J. Hübner, D. Hägele, W. W. Rühle, T. Hartmann, P. J. Klar, W. Heimbrodt, M. Lampalzer, K. Volz, and W. Stolz, Spin injection, spin transport and spin coherence, Semicond. Sci. Technol. **17**, 285 (2002).

[61] A. V. Kimel, A. Kirilyuk, P. A. Usachev, R. V. Pisarev, A. M. Balbashov, and T. Rasing, Ultrafast non-thermal control of magnetization by instantaneous photomagnetic pulses, Nature (London) **435**, 655 (2005).

[62] A. Kirilyuk, A. V. Kimel, and T. Rasing, Ultrafast optical manipulation of magnetic order, Rev. Mod. Phys. **82**, 2731 (2010).

[63] A. Altland and B. D. Simons, *Condensed Matter Field Theory* (Cambridge University Press, Cambridge, 2010).

[64] J. R. Schrieffer, *Theory of Superconductivity* (W. A. Benjamin, New York, 1964).

[65] F. Freimuth, S. Blügel, and Y. Mokrousov, Laser-induced torques in metallic ferromagnets, Phys. Rev. B **94**, 144432 (2016).

[66] F. Freimuth, S. Blügel, and Y. Mokrousov, Laser-induced torques in metallic antiferromagnets, Phys. Rev. B **103**, 174429 (2021).

[67] C. L. Kane and E. J. Mele, Quantum spin Hall effect in graphene, Phys. Rev. Lett. **95**, 226801 (2005).

[68] C.-C. Liu, W. Feng, and Y. Yao, Quantum spin Hall effect in silicene and two-dimensional germanium, Phys. Rev. Lett. **107**, 076802 (2011).

[69] C.-C. Liu, H. Jiang, and Y. Yao, Low-energy effective Hamiltonian involving spin-orbit coupling in silicene and two-dimensional germanium and tin, Phys. Rev. B **84**, 195430 (2011).

[70] X. Zhang, Q. Liu, J.-W. Luo, A. J. Freeman, and A. Zunger, Hidden spin polarization in inversion-symmetric bulk crystals, Nat. Phys. **10**, 387 (2014).

[71] J. Železný, H. Gao, K. Výborný, J. Zemen, J. Mašek, A. Manchon, J. Wunderlich, J. Sinova, and T. Jungwirth, Relativistic néel-order fields induced by electrical current in antiferromagnets, Phys. Rev. Lett. **113**, 157201 (2014).

[72] H. Watanabe and Y. Yanase, Chiral photocurrent in parity-violating magnet and enhanced response in topological antiferromagnet, Phys. Rev. X **11**, 011001 (2021).

[73] R. Peters, T. Pruschke, and F. B. Anders, Numerical renormalization group approach to Green's functions for quantum impurity models, Phys. Rev. B **74**, 245114 (2006).

[74] R. Bulla, T. A. Costi, and T. Pruschke, Numerical renormalization group method for quantum impurity systems, Rev. Mod. Phys. **80**, 395 (2008).

[75] M. Hohenadler, Z. Y. Meng, T. C. Lang, S. Wessel, A. Muramatsu, and F. F. Assaad, Quantum phase transitions in the Kane-Mele-Hubbard model, Phys. Rev. B **85**, 115132 (2012).

[76] M. Laubach, J. Reuther, R. Thomale, and S. Rachel, Rashba spin-orbit coupling in the Kane-Mele-Hubbard model, Phys. Rev. B **90**, 165136 (2014).

[77] A. M. Kalashnikova, A. V. Kimel, R. V. Pisarev, V. N. Gridnev, A. Kirilyuk, and T. Rasing, Impulsive generation of coherent magnons by linearly polarized light in the easy-plane antiferromagnet $FeBO_3$, Phys. Rev. Lett. **99**, 167205 (2007).

[78] F. Nastos, J. Rioux, M. Strimas-Mackey, B. S. Mendoza, and J. E. Sipe, Full band structure LDA and $k \cdot p$ calculations of optical spin-injection, Phys. Rev. B **76**, 205113 (2007).

[79] T. Kodama, N. Kikuchi, T. Chiba, S. Okamoto, S. Ohno, and S. Tomita, Direct observation of current-induced nonlinear spin torque in Pt-Py bilayers, Phys. Rev. B **109**, 214419 (2024).

[80] H. Watanabe, A. Daido, and Y. Yanase, Nonreciprocal optical response in parity-breaking superconductors, Phys. Rev. B **105**, 024308 (2022).

[81] D. J. Passos, G. B. Ventura, J. M. Viana Parente Lopes, J. M. B. Lopes dos Santos, and N. M. R. Peres, Nonlinear optical responses of crystalline systems: Results from a velocity gauge analysis, Phys. Rev. B **97**, 235446 (2018).